TÉCNICO LISBOA

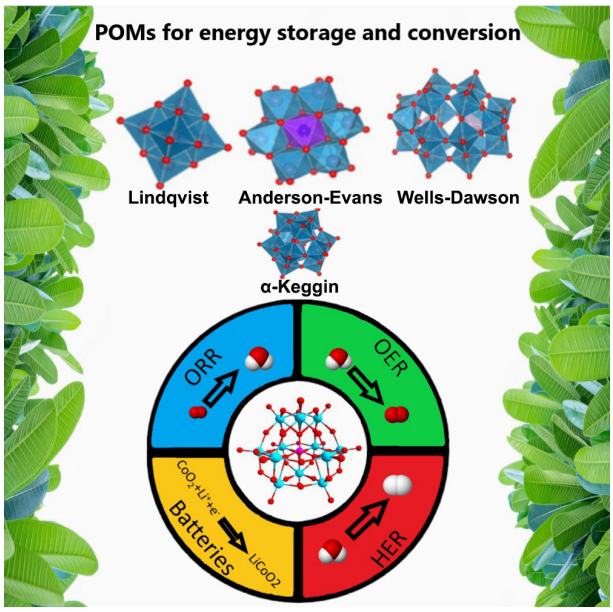

Composites of transition metal-polyoxometalates with reduced graphene oxide as efficient bifunctional electrocatalysts for metal-air batteries

Filipe Machado Botelho de Gusmão

Thesis to obtain the Master of Science Degree in

Chemical Engineering

Supervisor: Prof. Diogo Miguel Franco dos Santos
Prof. Biljana Šljukić Paunković

Examination Committee

Chairperson: Prof. José Nuno Canongia Lopes
Supervisor: Prof. Biljana Šljukić Paunković
Members of the Committee: Dr. Anup Paul

10/2022

Declaration

I declare that this document is an original work of my own authorship and that it fulfills all the requirements of the Code of Conduct and Good Practices of the Universidade de Lisboa.

Acknowledgements

To Professors Biljana Šljukić Paunković and Diogo Miguel Franco dos Santos for their competent guidance and support.

To my colleagues at the lab and from the Faculty of Physical Chemistry, University of Belgrade, Serbia for their generous collaboration.

To my mother and father for their encouragement and love.

Abstract

This thesis analyses the potential of polyoxometalates (POMs) as alternatives to noble metal-based electrocatalysts, further considering their contribution to face the challenges of upgrading modern energy systems into more sustainable ones.

As polyatomic ions with closed 3-dimensional frameworks, with many redox active sites, POMs have a specially interesting structure that could enable them to act as powerful electrocatalysts for electrochemical energy conversion and storage. They are cheaper and easier to obtain on a large scale than the noble metals electrocatalysts currently representing the most used ones in industrial electrochemical energy storage and conversion.

After reviewing POMs current use in batteries, supercapacitors, fuel cells, and electrolysers, fundamental studies were carried out for five transition-metal based POMs containing manganese, iron, cobalt, nickel and copper, all coordinated with reduced graphene oxide (rGO) to ascertain their viability as catalysts for the oxygen evolution reaction (OER), oxygen reduction reaction (ORR), and hydrogen evolution reaction (HER). For OER, the best material was found to be Ni-POM/rGO, for ORR it was Co-POM/rGO, and all of them were found not to be active for HER catalysis. Different POM:rGO ratios were also tested in order to optimise composition, and a ratio of 1:5 Ni-POM:rGO was found to be the most active for OER. Finally, metal-air batteries were built to optimise power density, again testing each POM to find out which is the most active. For the batteries, the best setup was using 4M KOH as electrolyte, and Co-POM/rGO as the catalyst.

Keywords: Polyoxometalates; Transition metals; Reduced Graphene Oxide; Metal-air batteries; Oxygen Evolution Reaction; Oxygen Reduction Reaction

Resumo

Esta tese analisa o uso de polioxometalatos (POM) como alternativas aos electrocatalisadores à base de metais nobres, considerando a contribuição da sua utilização para enfrentar os atuais desafios dos sistemas energéticos modernos para sistemas sustentáveis.

Por serem iões poliatómicos com estruturas tridimensionais fechadas, com muitos sítios activos redox, os POM têm uma estrutura especialmente interessante que os permite agir como poderosos electrocatalisadores para a conversão e armazenamento de energia por via electroquímica. São mais baratos e fáceis de obter em grande escala que os metais nobres actualmente utilizados como electrocatalisadores na indústria.

Após uma revisão da utilização de POMs em baterias, supercapacitores, células de combustível, e electrolisadores, foram realizados estudos fundamentais para cinco POMs à base de metais de transição contendo manganês, ferro, cobalto, níquel e cobre, todos coordenados com oxido de grafeno reduzido (rGO) para verificar a sua viabilidade como catalisadores da reacção de evolução do oxigénio (OER), reacção de redução do oxigénio (ORR), e reacção de evolução do hidrogénio (HER). Para a OER, o melhor material foi o Ni-POM/rGO, para ORR foi o Co-POM/rGO, e todos mostraram ausência de actividade para a catálise da HER. Várias razões Ni-POM:rGO foram testadas de forma a descernir a melhor composição, e a razão 1:5 Ni-POM:rGO foi a que maior atividade mostrou para a OER. Finalmente, foram construídas baterias metal-ar para optimizar a energia específica do sistema, testando novamente cada POM para identificar o mais activo. Para as baterias, a melhor configuração utilizou 4M KOH como electrólito e Co-POM/rGO como catalisador.

Palavras-Chave: Polioxometalatos; Metais de Transição; Óxido de Grafeno reduzido; Baterias metal-ar; Reação de produção de Oxigénio; Reação de redução do Oxigénio

Contents

List of Figures

List of Tables

Glossary

POM	Polyoxometalates
OER	Oxygen Evolution Reaction
ORR	Oxygen Reduction Reaction
HER	Hydrogen Evolution Reaction
EIS	Electrochemical Impedance Spectroscopy
CV	Cyclic Voltammetry
LSV	Linear Sweep Voltammetry
OCP	Open-Circuit Potential
SCE	Saturated Calomel Electrode
RHE	Reversible hydrogen Electrode
TOF	Turnover Frequency
KB	Ketjen Black
CNT	Carbon Nano-tubes
XRD	X-Ray Diffraction
FTIR	Fourier Transform Infrared Spectroscopy
SEM	Scanning Electron Microscope
E	Potential
i	Current
j	Current Density
ω	Angular Rotation Speed
P	Power Density
η	Overpotential
i_m	Measured current
i_K	Kinetic Current
B_L	Levich Constant
ν	Kinematic Viscosity
C	Concentration
c	Molar Concentration
n	Number of Electrons
F	Faraday Constant

A	Electrode Area
D	Diffusion Coefficient
C_{dl}	Double-Layer Capacitance
R_{ct}	Charge-Transfer Resistance
R_s	Electrolyte Resistance

Part I

Introduction

Chapter 1

Overview

Climate change is already taking its toll. At the 77th session of the UN General Assembly (UNGA 77) held in New York city from 13 to 27 September 2022, after visiting Pakistan, where devastating floods threw nearly 1/3 of the country underwater, affecting 33 million people, the UN Secretary-General defended that climate action must be the first priority of every Government, and Global greenhouse gas emissions must be reduced in 45% by 2030 to allow reaching net zero by 2050.

Nonetheless, despite all evidence that action must be taken, greenhouse gas emissions are expected to increase around 14% this decade [1].

Developing and putting in place industrial energy storage and production options that do not emit greenhouse gases should be priorities for all developed countries.

Important breakthroughs have been made in the field of renewable energy production, which is a significant part of the solution to curb greenhouse emissions, with major investments already in place in many countries across Europe. But sustainable renewable energy production relies on efficient energy storage, as its production varies widely throughout the day and the year. Efficient energy storage guarantees that this energy becomes available in a way consistent with demand.

Using hydrogen as an energy carrier is a good option already in use. Even if most hydrogen currently comes from hydrocarbon reforming, a major source of greenhouse gas emissions, green hydrogen gas can be produced using electrolysis cells powered by renewable energy sources. Adding to this, hydrogen can be fed to fuel cells to generate electricity.

However, scaling up this technology to industrial levels has proven to be difficult. As oxygen evolution reaction (OER) has slow kinetics, it requires high overpotentials for reasonable currents to develop, and the electrocatalysts typically used to reduce the electrical uptake of this reaction are made of high-cost and rare materials such as iridium and ruthenium. The best performing low-cost catalysts normally operate in current ranges below 100 mA cm^{-2}, which are unsuitable for industrial use. The study of low-cost and high-performing catalyst materials is also difficult. Since it is usually conducted in small-scale lab cells, the conditions of temperature, pressure, and electrolyte concentration values are bound to differ when scaling up to industrial cells, giving rise to significant divergences in electrolyte conductivity, ion migratory flux, and catalyst structural stability [2].

POMs, on the other hand, have shown high thermal stability, high sensitivity to electricity, and resistance to oxidative decomposition when used in catalysis, making them prime options for electrocatalytic study. Although POM-salts are mostly insulators, it is now possible to attach POMs to conductive and high-surface area materials through covalent or non-covalent means, using materials generated by nanostructured conductive carbons such as carbon nano-tubes (CNTs) and graphene [3]. "Wiring" of POMs to conductive organic polymers has also been suggested as a way to overcome the issue of their low conductivity [4]. It seems possible, then, to overcome POMs low conductivity, and produce reliable electrical connection between the POM as the reaction centre and other parts of the device, thus enabling the technological use of POMs in electrical devices.

POMs have exhibited the potential for multi-electron transfer, with their unique redox properties allowing the reversible uptake of up to 24 electrons per cluster unit (for example: $[PMo_{12}O_{40}]^{3-}$), which has been observed in the solid state [4, 5, 6, 7, 8, 9]. Furthermore, their exact electrochemical properties such as redox potentials and number of stored electrons can be manipulated by chemical modification of the POM structure, one of the methods available being the incorporation of redox-active metal centres in them. Metal functionalization can also be used to generate coordinative substrate binding sites for electrochemical and electroanalytical applications [4].

Finally, there is already a large body of knowledge around these materials and applications in material and medical sciences are currently in place, supporting the potential scalability of these materials to industrial levels.

POMs have thus interesting properties for OER, ORR, and HER electrocatalysis, with potentially good activity, low cost, and scalability. This study aims at exploring the use of six transition-metal based POMs containing Manganese, Iron, Cobalt, Nickel and Copper as electrocatalysts for OER, ORR, HER electrocatalysis and as catalyst for metal/air batteries, while also addressing their potential to overcome the problems encountered with other materials in the search for an efficient production and storage of green hydrogen in industry.

To that end, we first reviewed the existing research on these materials as electrocatalysts for the OER, ORR and HER reactions, and their use in batteries and supercapacitors. We then proceed to study five synthesized POM-transition metal hybrids. The synthesized POMs were characterized according to their structure, diffraction data, surface functionality, surface morphology and atomic composition. They were tested as catalysts for OER, HER, ORR and as a catalyst for metal-air batteries. We then discuss the results obtained, comparing their behaviour and cost with the most commonly used materials. We further conclude which one performs best.

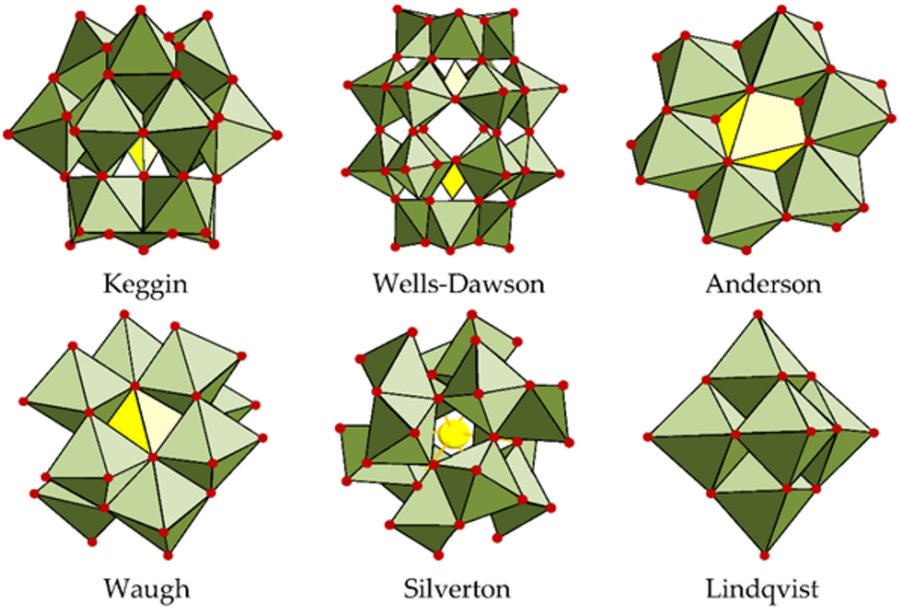

Figure 1.1: POM structures in polyhedral representations (adapted from [10]).

Chapter 2

Theoretical introduction

To carry out the necessary measurements, it is important to understand the underlying concepts through which they can be interpreted. Considering firstly the cell system, it is composed of 3 electrodes, a working electrode on whose surface the catalyst is deposited, a counter electrode, and a reference electrode, the system is also filled with a conducting electrolyte.

By inducing a potential difference in the working electrode vs. the counter electrode, the relevant chemical reaction can be observed, as a function of the resulting electrical current. And as a first approach, it can be assumed that the higher the catalytic activity of the material for a given reaction, the higher the resulting current, for the same value of potential difference. This is the basis for voltammetry, by sweeping a given potential range, a graph can be plotted showing current peaks at the potentials at which reactions take place.

In a more in-depth analysis, several factors are analysed to compare different catalysts. Namely, for the OER, onset potential is the potential at which a current density of 1 $mAcm^{-2}$ is achieved. 10, the overpotential at which a current of 10 $mAcm^{-2}$ is reached. j_{400}, the current at an overpotential of 400 mV. And finally, Tafel slope is the value of the potential increase necessary to multiply the current output tenfold.

Another important measurement to be done is potentiostatic electrochemical impedance spectroscopy (EIS). The resulting Nyquist plot can be interpreted to obtain the values of the different resistances in the system, such as the charge-transfer resistance, electrolyte resistance, and diffusion layer resistance.

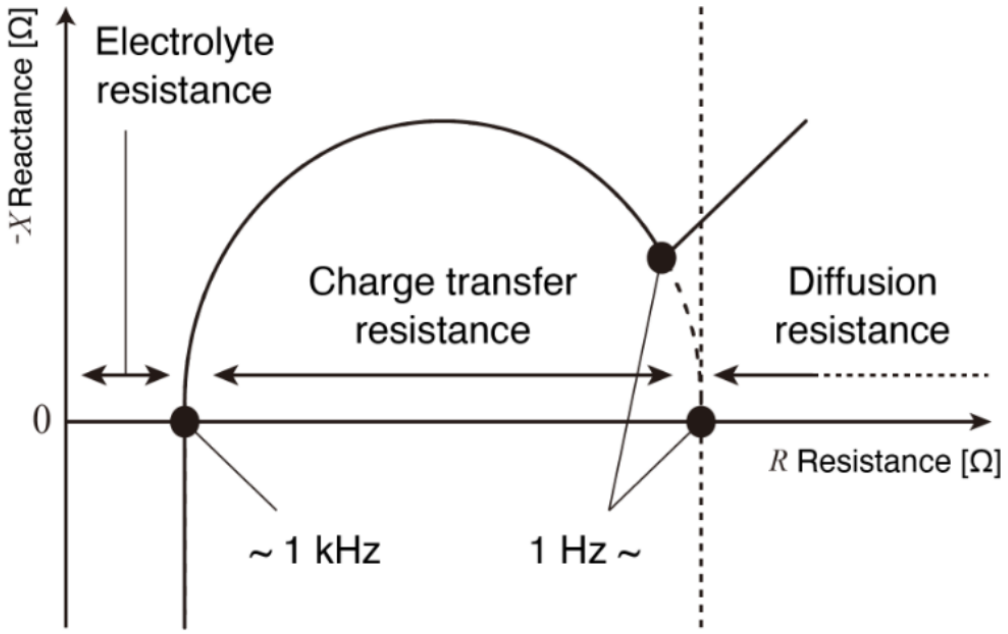

Figure 2.1: Representation of Nyquist plot from EIS (adapted from [11]).

In some cases, when plotting data from cyclic voltammetry (CV) and linear sweep voltammetry (LSV), an ohmic drop correction needs to be made. The correction is necessary due to the electrolyte resistance between the working electrode and reference electrode, which causes the measured potential difference to be higher than the actual difference between electrodes. This is particularly important if the electrolyte is not very conductive or the measured currents are fairly high. The correct graphs for LSV can be plotted by applying the following equation to all the measured potentials.

$$V_{corrected} = V_{measured} - iR \tag{2.1}$$

As for metal-air batteries, they are composed of a pure metal anode, ambient air as the cathode, and an electrolyte. These types of batteries, using a bi-functional electrocatalyst, can be rechargeable. During discharge atmospheric O_2 is reduced in the cathode, while the metal is oxidised to its ionic form. During recharge, the exact opposite process takes place.

Metal-air batteries are promising due to having high energy density, while also being safer, added to this, the fact that this type of batteries uses atmospheric air as cathode makes them significantly lighter and cheaper than other models. To determine the best configuration of a metal-air battery, power density curves are used. By comparing which of the set-ups has the highest maximum of the curve, the best can be found.

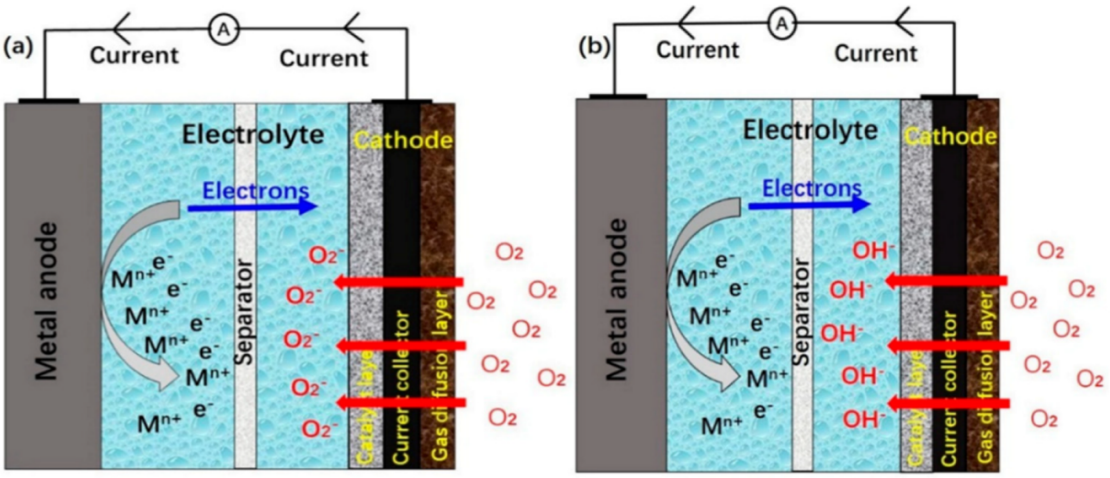

Figure 2.2: Metal-air battery operation for (a) non-aqueous electrolyte and (b) aqueous electrolyte (adapted from [12]).

To study the ORR, Koutecký-Levich analysis is necessary. This is done as a way to measure the current obtained from the electrochemical reaction as a function of the kinetic activity and mass transport of the reactants.

$$\frac{1}{i_m} = \frac{1}{i_K} + \frac{1}{B_L \omega^{0.5}} \tag{2.2}$$

Where B_L is the Levich constant:

$$B_L = (0.620) n F A D^{\frac{2}{3}} \upsilon^{\frac{-1}{6}} C \tag{2.3}$$

By recording CVs at different rotation rates, a Koutecký–Levich plot can be drawn. Plotting reciprocal current vs. the reciprocal square root of the rotation rate for a specific potential, a linearization is made. The kinetic current can then be determined, and by calculating the number of exchanged electrons from the Levich constant equation, the preferential pathway of the reaction can be discerned.

Chapter 3

State-of-the-art

POMs as electrocatalysts for the oxygen evolution reaction (OER)

The oxygen evolution reaction (OER) is the process by which the water is oxidized to O_2 in water electrolysis. It is agreed that this is a good option to produce green hydrogen, but although the mechanisms of this reaction differ with the pH of the electrolyte solution, both have high thermodynamic demands and kinetic obstacles which translate to hogh activation energies. These are so high that the overpotentials needed to start the reaction are not sustainable in the long term for application in the production of commercially available electrolysis cells. This uncovers the necessity to research and develop more efficient catalysts, that allow this sustainability to hold.

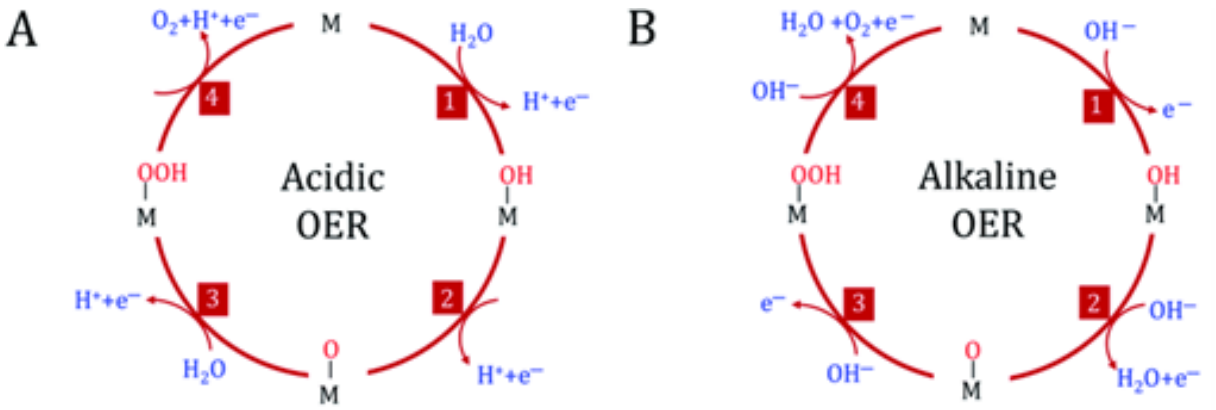

Figure 3.1: Conventional OER mechanism for acidic and alkaline conditions (adapted from [13]).

Luckily, there are currently promising results for using POMs as catalysts for the OER [10], specifically lacunary POMs, obtained by removing metal oxygen entities in the POM structure, thus creating empty spaces. These lacunary POMs can sustain a robust structure because, being good inorganic ligands, they can stabilise multi-metal oxide clusters. This strong structure can serve as a basis for catalytically active transitional metal-oxo clusters. Varying the metals serving as active sites allows the study and comparison of the catalytic effect among different POMs.

Ruthenium POMs

Although ruthenium (Ru) is a noble and therefore very expensive metal, it is one of the transition metals that can act as an active site for the POMs. It has been found Ru is a powerful oxidant in near neutral pH. (Ru_4Si_2) is, in fact, highly active for this reaction [14, 15], having a ratio of product formed per molecule of catalyst (TON) of up to 180 and initial d(TON)/dt (TOF) of up to 288 h^{-1}[16]. (Ru_4P_2) was also shown to be able to catalyse the OER, but at a slightly lower efficiency.

Other studies show that anchoring Ru_4Si_2 to a conductive bed of multi-walled carbon nano-tubes (MWCNTs) allows for higher electrocatalytic activity when compared to Ru_4Si_2 functionalised amorphous carbon. These results could be explained by the enhancement of electron transfer in MWCNTs. With MWCNTs, a TOF of 300 $h^{-1}$was reached at an overpotential of 0.6 V [17].

Guo et al. [18] found that composite materials, based on electrostatic immobilisation of Ru_4Si_2 onto graphene followed by electrochemical deposition on glassy carbon, had good catalytic activity and stability under near neutral pH, showing an overpotential of 0.35 V.

Quintana et al. [19], found that using graphene, covalently functionalised with organic hydrogen-bonding cations also enhanced significantly the electrocatalytic performance of Ru_4Si_2, enabling higher efficiency than both isolated Ru_4Si_2 and its nano-tube analogue. This hybrid material has shown an overpotential as low as 0.3 V and negligible performance loss even after 4 hours of testing, all at neutral pH.

Cobalt POMs

Cobalt (Co) is more common than Ru, so also less expensive, although not particularly more sustainable. Co reserves are located in countries with few regulations, with known practices of workers exploitation and lack of supervision and treatment of the mining industry's pollutants [20]. So, Co may be considered a midway between the more sustainable transition metal-based POMs and the noble metal-based materials.

Limani et al. [21] tested the feasibility of four Cobalt phosphotungstate materials (MWCNT_N8_Co4, GF_N8_Co4, GF_ND8_Co4, and GF_NS8_Co4) as electrocatalysts. All materials showed good performance, in alkaline media (pH=13), particularly GF_N8_Co4, which had an onset potential of 0.34 V vs. RHE and a maximum current of 70 mA cm^{-2} at 2 V vs. RHE, while also maintaining around 73 to 82 % of its current after 5.5 hours. These results show that this electrocatalyst has the potential to outperform state-of-the-art IrO_2.

Manganese POMs

Manganese (Mn) is a more sustainable alternative than Ru and Co, due to being in more abundance in the earth's crust. Unfortunately, there are not many studies with Mn-POMs. Perhaps this relates to Mn oxide being much less active than the corresponding Co or Ni analogues, even when considering heterogeneous catalysis [22].

Amongst the Mn-POMs that exhibit OER activity, a good candidate to experiment with seemed to be the Mn-analogue of the well-studied Co_4P_2, (Mn_4) [23]. Unfortunately, despite an initial activity comparable to Co in electrochemical water oxidation experiments, the current density decreased very rapidly, becoming negligible in 30 min, with the formation of an inactive MnOx layer on the electrode.

Wu et al. [24] tested six solutions of different Mn-POMs, depositing electrodes on an indium tin oxide surface to form the composite. The Mn-POMs studied were: (Mn_2-POM), (Mn_4-POM), $(Mn_6-POM-1)$, $(Mn_6-POM-4)$, $(Mn_{14}-POM)$, $and (Mn_{19}-POM)$. The authors concluded that Mn14-POM displayed the highest electrocatalytic performance towards OER and that there were two main factors impacting the electrocatalytic performance for this reaction, namely the oxidation state of Mn and the structure of Mn-O cluster cubic structure.

Nickel POMs

Nickel POMs are some of the most recent ones to be studied, for example, (Ni_5Si_2) was only first reported in 2012, by Zhu et al. [25]. Singh et al. [26] reported a hybrid POM-supported Ni^{II}coordination complex, $[(Ni^{II}(bpy)_2(H_2O))(HCo^{II}W_{12}^{VI}O_{40})]^{23-}$, with Ni^{II} metal ion acting as the active centre, which was highly stable and robust for OER at pH 7. It also showed a high TOF of 18.49 (mol of O_2)(mol of $Ni^{II})^{-1}$ s^{-1} and a Tafel slope of 168.41 $mV\,dec^{-1}$.

Copper and Iron POMs

Yu et al. [27, 28] tested two Cu-POMs clusters, where $[Cu_3(H_2O)_3(SbW_9O_{33})_2]^{12-}$ was shown to catalyse OER at neutral pH without decomposition, under homogeneous electrochemical conditions. On the other side, $[Cu_5(OH)_4(H_2O)_2(SiW_9O_{33})_2]^{10-}$ showed negligible electrochemical activity under the same conditions. This last result is somewhat surprising as this was the POM found to be able to photochemically catalyse the same reaction. Azmani et al. compared Fe-POMs and Co-POMs, specifically, (Fe4-WS) and (Co4-WS) were tested. The authors found that CoII-POMs have better OER activity than the Fe^{III} counterparts. These results are in line with the theory, as the lower Tafel slope displayed by Co4-WS indicates faster kinetics than Fe4-WS, which correlates well with the lower activation barriers found for Co4-WS. [29]

Han et al. used sub-nanometre heterometallic CoW and FeCoW clusters, constructed via a molecule-to-cluster strategy by using different POMs (i.e., $[(Co_4(OH)_3PO_4)_4(SiW_9O_{34})_4]^{32-}$, $[(Fe_2Co_2(OH)_3PO_4)_4(SiW_9O_{34})_4]^{24-}$, and $[(FeCo_3(OH)_3PO_4)_4(SiW_9O_{34})_4]^{28-}$) as precursors. The most efficient system studied had excellent OER activity with η_{10} = 192 mV and a low Tafel slope of 36 mV dec^{-1}. Interestingly, in this study, the Fe content in the FeCoW clusters could be controlled by using POM precursors containing different numbers of Fe atoms. [30]

POMs as electrocatalysts for the hydrogen evolution reaction (HER)

Though the OER is the efficiency-limiting process in electrolytic water splitting, the hydrogen evolution reaction (HER), which involves several steps [31] also poses some challenges that must be tackled. As stated before, hydrogen production is currently a possible solution to the world's current energy problems, but existing platinum electrocatalysis solutions need to be replaced by lower-cost alternatives. POMs are potential candidates as catalysts for green hydrogen production. They have been shown to have close enough properties to commercial carbon-supported platinum (Pt/C), the most used catalyst for acidic and

alkaline media, while being considerably cheaper.

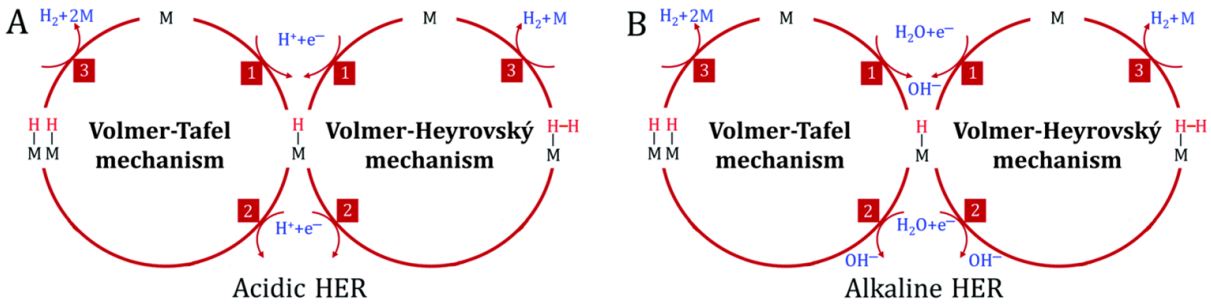

Figure 3.2: Schematic illustration of the hydrogen evolution reaction mechanism in acidic and alkaline media.

Singh et al. [32] found an overpotential of 520 mV and a turnover frequency (TOF) of 6329 mol of H_2 evolved per mole of Cu atom, per hour, at the current density of 1 mA cm^{-2} when testing copper-based POM $[Cu^{II}(2,2-bpy)(H_2O)_2]\,[Co^{II}W_{12}^{VI}O_{40}Cu^{II}(2,2-bpy)(H_2O)Cu^{II}(2,2-bpy)]\cdot 2H_2O$, close to neutral pH. In this POM $Cu^{II}(2,2-bpy)(H_2O)_2{}^{2+}$ acted as the active centre, catalysing the HER. These results represent a major leap in efficiency when compared with previously tested Cu clusters, which displayed a TOF of 457 mol of H_2 per mol of catalyst, per hour, at 817 mV [33] and even with the Ni and Co complexes, found to have values of 970.45 and 871.17 mol of H_2 mol $catalyst^{-1}h^{-1}$, respectively, requiring an overpotential of 837 mV. [34, 35].

Recently Wang et al. [12] tested the electrocatalytic properties of three other copper-based POMs, namely the following POM-based metal-organic complexes: $Cu_2(3-bptzp)_3(H_2O)_4[SiW_{12}O_{40}]\cdot H_2O$, $Cu_2(3-bptzpe)_2(H_2O)_8[SiW_{12}O_{40}]\cdot 4H_2O$, $and\,Cu_2(3-bptzh)_3(H_2O)_6[SiW_{12}O_{40}]$, where (3-bptzp = 1,4-bis (5-(3-pyridyl)- tetrazolyl)- butane; 3-bptzpe = 1,4-bis(5-(3-pyridyl)tetrazolyl)- pentane, and 3-bptzh = 1,4-bis(5-(3-pyridyl)tetrazolyl)-hexane). The authors found that they all showed good electrocatalytic activity under alkaline and acidic media. $Cu_2(3-bptzp)_3(H_2O)_4[SiW_{12}O_{40}]\cdot H_2O$, the best performer, displayed a current density of 10 mA cm^{-2} at an overpotential of 59.4 mV vs. RHE, leading to a Tafel slope of 74.2 mV dec^{-1} .

All these POMs were found to be stable under the full pH range, although interestingly enough, acidic media led to higher overpotentials together with lower impedance.

Fernandes et al.[36] developed and tested three further POMs in acidic media. The nanocomposites were inserted into POMs on reduced graphene oxide (rGO), and all of them displayed similar overpotentials to that of the best commercial Pt/C. P2W18@rGF_ox, P5W30@rGF_ox, and P8W48@rGF_ox were prepared by an easy and cost-effective method involving one-step electroreduction of POM@rGF_ox. P5W30@rGF_ox showed the best activity with a Tafel slope of 33 mV dec^{-1} , but even the worse one, P8W48@rGF_ox, had a Tafel slope of 41 mV dec^{-1} , which is relatively close to that of commercial Pt/C, 30 mV dec^{-1} .

Yang also developed and tested a dual-atom catalyst consisting of O-bridged W-Mo atoms anchored to N-doped graphene vacancies through oxygen atoms with W-O-Mo-O-C configuration [37]. The material was synthesized by controlled self-assembly followed by nitridation and, in testing conditions, exhibited

Pt-like activity and high stability for HER across the pH scale. The material was shown to be more active than similarly structured Mo–Mo and W–W homodimer catalysts.

Another material, in this case a heterostructure of zinc iron oxide ($ZnFe_2O_4$) and polyoxometalate (POM) nanoplates (POM–$ZnFe_2O_4$), fabricated for the first time by a hydrothermal process [38], showed overpotentials of 268 and 356 mV, and 220 and 290 mV to achieve current densities of 20 and 50 mA cm^{-2}, in the HER and OER analysis, respectively. Adding to these results, an electrolytic cell composed of a POM–$ZnFe_2O_4$ cathode and anode was shown to require a cell potential of only 1.53 V to deliver a current of 10 mA cm^{-2}.

This is a better electrochemical performance than both the commercially used and the most recently reported catalysts. This behaviour could be explained, according to the authors of the study, by the high electrocatalytically active surface area, the modulation in the electronic and chemical properties, and the formation of heterojunction of $ZnFe_2O_4$ and POM, which are vital for accelerating HER and OER activity.

All these studies on POMs for HER show excellent potential for this class of compounds. They also encourage further work in other materials to be combined with the POMs, creating highly conductive nanocomposites.

POMs as electrocatalysts for the oxygen reduction reaction (ORR)

The presence of transition metal ions in the POM framework enables fine-tuning of their redox potentials. Incorporating a POM-based catalyst can increase the rate of the electroreduction process and lower the overpotential. The POM is said to “act as a powerful electron reservoir” and usually can provide electrons to other species [39].

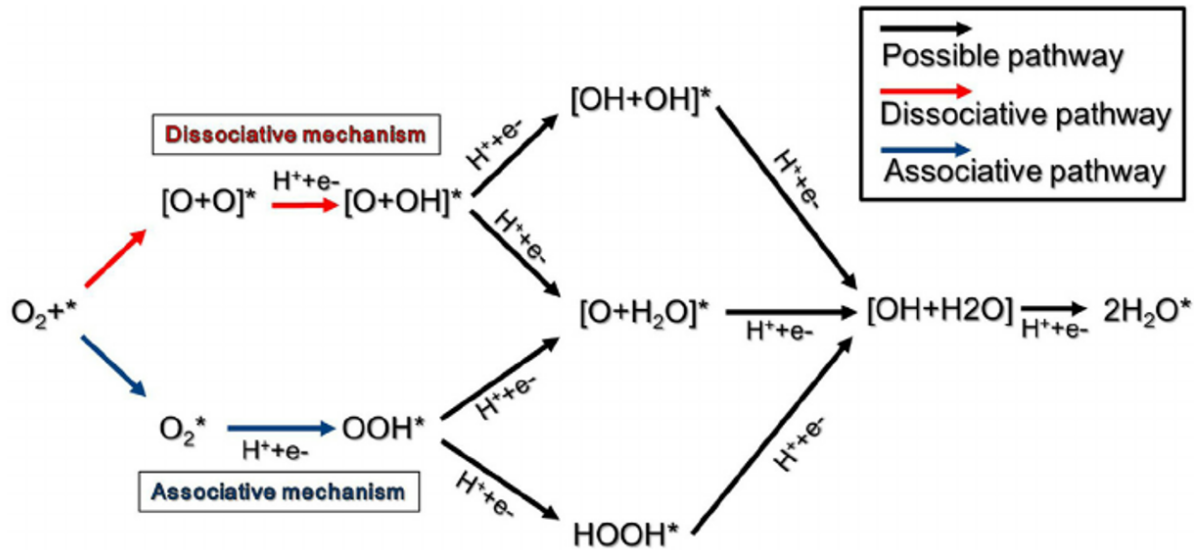

Figure 3.3: ORR Mechanism.

The oxygen reduction reaction (ORR) is an integral part of fuel cells and metal-air batteries. So, to create good catalysts low overpotential of the reaction is necessary, but there is more to consider.

Ideal electrocatalysts, if we are looking for optimal running of rechargeable metal-air batteries or unitised regenerative fuel cells, should also be bifunctional, that is, they should be active for both OER and ORR. Further, it would be important that they were resistant to methanol crossover, to allow their used in direct methanol fuel cells. Finally, although currently used catalyst for ORR applications have a 4-electron transfer mechanism, where O_2 is reduced to form water, according to Zheng et al. [40] the 2-electron transfer pathway can sometimes be desirable, as a safer and cheaper way to produce H_2O_2 than current technology.

Zhang et al. [41] reported on the efficiency of several supports for Ni and Co POM core. The supports were thermalized triazine-based frameworks (TTFs), fluorine-doped TTF (TTF-F), and rGO. In this study $(PW_9)_2Ni_7\}/Cu(ethylenediamine)_2/TTF-F$ was found to be the first POM-based noble metal-free ORR catalyst that displayed comparable ORR activity to Pt/C and much better stability in neutral medium. At this pH, $Cu_6Ni_7/TTF-F$, Cu_6Ni_7/rGO, and Cu_6Ni_7/C were the first examples of POM-based electrocatalysts able to promote the one-step reduction of oxygen to water. Overall, all materials compared favourably to commercial Pt/C.

Liu et al.[42] have recently produced another POM that showed excellent performance for electrocatalytic ORR, in part superior to a commercial Pt/C. The material was obtained using a novel top-down POM-based single atom catalyst design [DS3]. The authors found that immobilization of POM-single site catalysts on high surface-area electrically conductive carbon could be achieved at high loading [43]. The Keggin-polyoxomolybdate$[PMo_{12}O_{40}]^{3-}$ was used by the authors as a precursor to deposit POM-like molybdenum (VI)-oxo subnanometer clusters ([Mo-oxo]n, n = 1–20) on high surface-area mesoporous carbon.

Marques et al. [44] studied three Fe and Ni-based POMs on MWCNTs, $(Na_{12}[(FeOH_2)_2Fe_2(As_2W_{15}O_{56})_2]\cdot 54H_2O$, $Na_{12}[(NiOH_2)_2Ni_2(As_2W_{15}O_{56})_2]\cdot 54H_2O$ and $Na_{14}[(FeOH_2)_2Ni_2(As_2W_{15}O_{56})_2]\cdot 55H_2O)$, in alkaline media. All showed good ORR performances, with onset potentials of ca. 0.80 V vs. RHE and diffusion-limited current densities between −3.19 and −3.66 mA cm^{-2}. Stability tests showed Fe4@MWCNT_N6 and Fe2Ni2@MWCNT_N6 to be the most promising, maintaining 84 and 80 % of current, respectively, after 12 h. Also, the number of electrons transferred per molecule of O_2 was close to three, suggesting a mixed regime.

Another study showed that RuPOM is an efficient OER/ORR bifunctional catalyst [45]. This material exhibited a bifunctional activity comparable to commercial Pt/C catalysts, when incorporated with conducting Ketjenblack (KB) carbon. RuPOM was more efficient in OER and slightly less efficient in ORR than Pt/C. but the material was much superior to Pt/C when comparing the specific activity of catalysts per precious metal used. The best performing RuPOM/KB (8:2 mixture) exhibited 25 and 11 times higher specific activity than RuO_2/KB and Pt/C, respectively, for ORR. By employing RuPOM/KB as a bifunctional OER/ORR catalyst, the performance of SWBs was significantly improved. The potential difference between charging (with OER) and discharging (with ORR) process was reduced from 1.30 to 0.76 V, and the output power was significantly enhanced.

Limani et al. [21] found good ORR performance of $MWCNT\_N_8\_Co_4$, $GF\_N_8\_Co_4$, $GF\_ND8\_Co_4$, and GF_NS8_Co4. These materials had onset potentials from 0.83 to 0.85 V vs. RHE, good tolerance

to methanol crossover, with current retention between 88 and 90%. They also displayed good stability after 20,000 s at 0.55 V vs. RHE, maintaining between 73% and 82% of initial current. The number of electrons transferred per O_2 molecule was close to four, implying selectivity for the direct process.
As has been described, in addition to their lower cost and greater availability than noble-metals currently used as electrocatalysts in industry, a variety of POM-based materials shows good activity for the reactions required for water splitting technologies, both in hydrogen production for energy storage, and as a bifunctional catalyst in OER and ORR. We can thus conclude that POMs are very interesting materials to be used for the construction of batteries and supercapacitors. The research on this subject will be reviewed in the next chapter.

POMs for batteries and supercapacitors

One of the most critical challenges for energy storage today is the development of high-performance, rechargeable, low-cost, and environmentally friendly batteries. To improve their design, new electrode materials, that can lead to higher cell potentials and higher capacities, but also that are produced with low environmental impact themselves, need to be discovered. POMs have been directly linked to stepping forward in solving this challenge.

Lithium-ion batteries

One of the most common energy storage methods today is the lithium-ion battery (LIB). This material is widely used due to its high cell potential, high energy density, and long-life cycle. In commercial cells, the most common cathode materials for this type of battery are lithium transmission metal oxides such as $LiCoO_2$, $LiMn_2O_4$, and $LiFePO_4$, and the most common anode is Graphite. But Graphite has low capacity and therefore limits the viability of using these batteries in large-scale systems. Also problematic is the decrease in the capacity of cathode [DS4] materials during cycling, not to mention the scarcity (and therefore high cost) of some of the components of these batteries, especially cobalt.
Vast amounts of resources are being channelled to the research of new materials for this type of batteries. POMs have received some interest in this field because, even though they have low electrical conductivity, usage of nanosized particles and/or mixing them with conductive materials can improve their properties. Additionally, POMs molecular clusters show multielectron redox as individual [DS5] [FMBdG6] [DS7] molecules, making their cycling stability and capacity independent of their crystalline stability [46]. They are also considerably easier to obtain and have a much lower cost than their counterparts.

Sodium-ion batteries

Sodium-ion batteries (SIBs) are a promising, relatively new technology for large-scale energy storage applications. SIBs rely on the large abundance of sodium, along with the use of low-cost aluminium as a current collector for both anode and cathode materials. The use of sodium in this type of cells is possible because, unlike lithium, it does not alloy with aluminium. SIBs energy density is lower than LIBs, though. This happens for three reasons: the large radius of the Na^+ ions, the larger atomic weight of sodium when

compared to lithium, and its low operating potential [47].

The use of new cathode and anode materials has been studied at length in the search for solving this problem. Liu et al. [48], and Chen et al. [49] tested POM-based materials for cathodes, while Hartung et al. [50] and Lin et al. [51] focused on anode materials. The main conclusion of all these studies is that, in fact, storage capacities in SIBs were much lower than in LIBs. Low kinetics, resulting from a passivation layer of Na_2O, forming during the first charge/discharge cycles has been proposed as a possible cause for these findings, pointing at yet another direction for research.

Redox flow batteries

Redox flow batteries (RFBs) are an emerging technology shaped for stationary machines. Unlike conventional secondary batteries, where the electrolyte is inside the cell involving the electrodes, RFBs use two electrolytes containing different electroactive species, the anolyte, and the catholyte, stored outside the cell and continuously pumped in [52]. The two electrolytes are separated by a membrane that acts both as a barrier, not allowing direct mixing, and as a transporter of charged ions between the electrolyte solutions. The modular design allows the cell to be sized as required and thus able to be used in all the range of energy and power demands of the market. This feature makes this kind of batteries very promising for industrial usage.

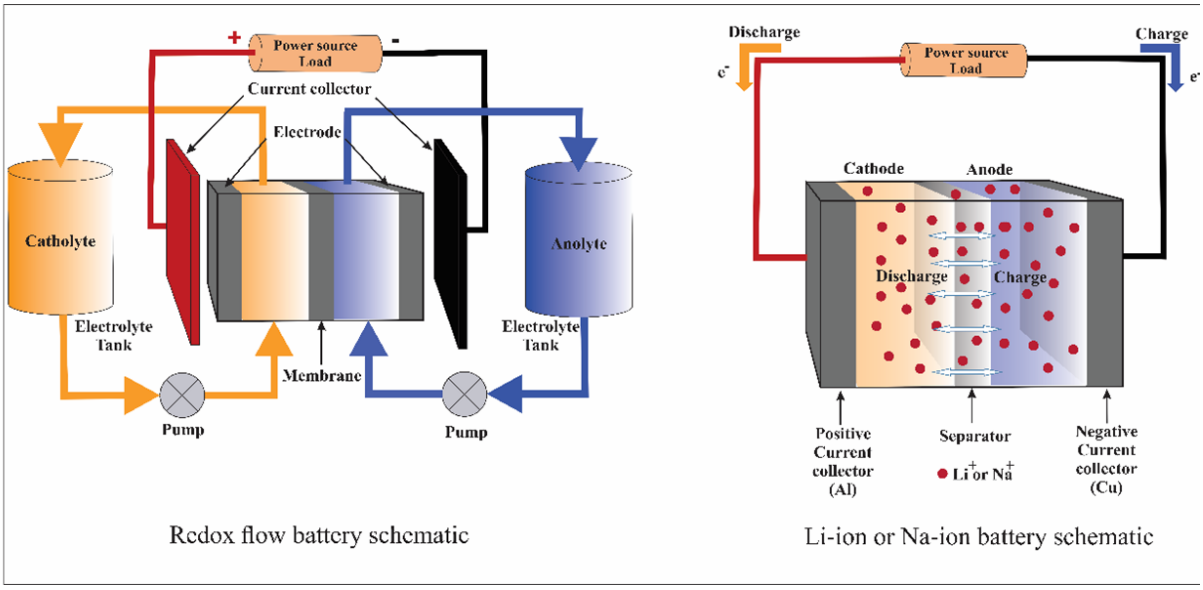

Figure 3.4: Scheme of a redox flow battery (adapted from [53]),and metal (Li, Na)-ion battery.

Engineers at NASA were the first to propose the concept of these batteries in the 70s, but research led to limited cycling stability and excessive hydrogen production. Nevertheless, several redox-active species have been tested throughout the years, with different levels of success [54, 55, 56].

In this context POMs have been tested as possible enhancers of the RFBs electrochemical parameters. Pratt et al. [57] assembled three phosphorus-based POMs ($A-a-PV_3W_9O_{40}^{6-}$, $B-a-PV_3W9O_{40}^{6-}$, $and\ P_2V_3W_{15}O_{62}^{9-}$) for use in the electroactive electrolytes of the RFBs. The authors found good pairs of electroactive species (positive and negative), such as ($P^{VI}V_3W_9^{VI}O_{40}^{9-}/P^{V}V_3W_9^{VI}O_{40}^{6-}$) and

($P^{VI}V_3W_9^{VI}O_{40}^{9-}/P^{VI}V_3W_3^{V}W_6^{VI}O_{40}^{12-}$).

The research, however, hasn't yet been able to surmount the low coulombic efficiency and poor cycling stability of POMs, problems that must be solved for POMs to be used in RFBs.

The hybridization of POMs with other materials has also been proposed in this context, as a possible way to increase their electrochemical activity. Dubal et al. [58] tested the hybridization of graphene and POMs, and found that rGO/phosphomolybdate-based RFBs showed good electrochemical features, namely a specific capacitance of 305 F g^{-1} as well as strong coulombic efficiency (77–79%) after 2000 cycles. Even though these results are still below the vanadium counterparts, they open the door for more research that could lead to breakthroughs in using POMs as electroactive species for use in electrolytes for RFBs.

Supercapacitors

Supercapacitors (SCs) store charge via the electric double layer; high surface area leads to charge storage due to the electrophysical separation over very small distances at the electrode-electrolyte interface. Their main goal is to deliver very high-power densities, at the expense of energy density. Graphene is the material used by excellence, representing a 100% exploited atomically thin surface, for the formation of the electric double layer[59].

Supercapacitors are thus used in vehicles, buses, trains, cranes, and elevators, where many rapid charge/discharge cycles are needed, rather than long-term compact energy storage. In these devices, they deliver burst-mode power, allow regenerative braking and short-term energy storage. For supercapacitors to be used more widely and efficiently, one of the fundamental challenges still to overcome is the limited amount of energy they can store. Further, this higher storage capacity must be achieved without losing their high-power capability and long cycle life.

Pursuing the goal of maximum energy density, research has been focused on the search for the best double-layer materials, and it has achieved capacitances as high as 200–300 F g^{-1}. [60] Nonetheless, there may exist other interesting paths the research can take. For instance, improving the extrinsic pseudocapacitive behaviours of materials, in which active species undergo fast reversible redox reactions close to the electrode surface, is also an excellent means of improving energy density [61].

POMs seem great contenders for this pseudocapacitance given their high surface-to-bulk ratio and their metal species' significant number of available redox states.

Vanadate POMs have already been used as positive electrodes in the construction of asymmetric cells.Using activated carbon as the negative electrode, a capacitance of 354 F g^{-1} was reported, as well as specific energy of 73 W h Kg^{-1} at 0.1 A g^{-1} and an associated power of 312 W Kg^{-1} [62].

Gupta et al. [63] studied the possibility of using hybrids of phosphomolybdate acid ($H_3PMo_{12}O_{40}$) and phosphotungstic acid ($H_3PW_{12}O_{40}$) with rGO in supercapacitators. The hybridization's effect on the electrochemical properties of the POM had very positive results. The specific capacitance increased from 70 F g^{-1} to 350 F g^{-1} for pure rGO, and a higher current carrying capacity was also achieved while maintaining good retention (94 %), resulting in higher specific energy and specific power density.

There are nonetheless still some challenges regarding the use of these materials in supercapacitators. For example, POMs need to be securely anchored to a host material to achieve long-term cycling stability.

Methodological issues also contribute to making the research more complex, as a great variability of metrics is used to express results making it harder to compare different studies and materials [46].

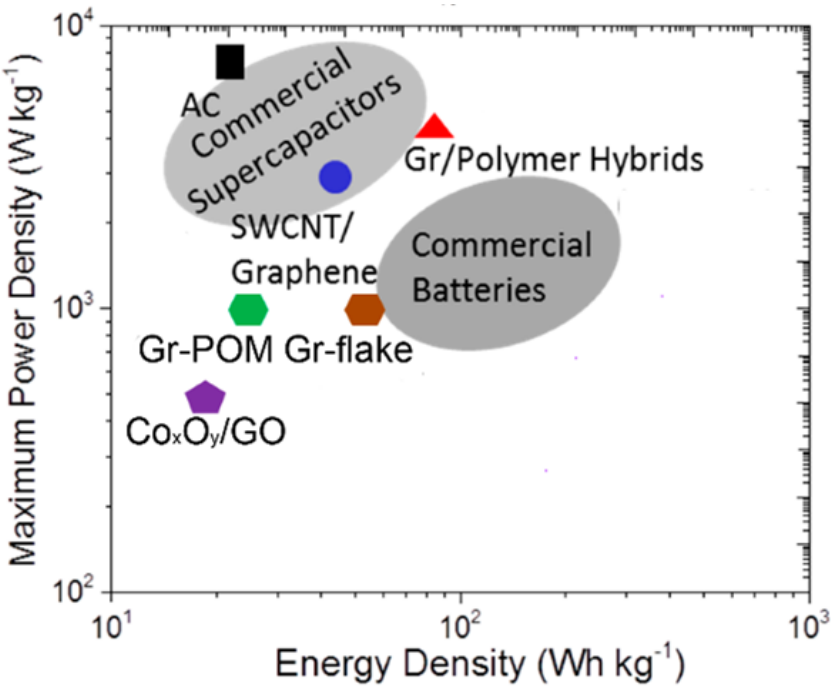

Figure 3.5: The performance of commercial supercapacitors and batteries, activated carbon, carbon nano-tube/graphene, graphene–polymer hybrids, and graphene–POM electrodes (adapted from [64]).

Part II

Experimental procedure

Synthesis and characterization of POMs and their composites with rGO

The materials were prepared in collaboration with the Faculty of Chemistry and Faculty of Physical Chemistry, University of Belgrade, Serbia. All of them were synthesised using a procedure similar to the one proposed by Clemente-Juan et al. [65] 22 mM solutions were prepared for five compounds, dissolving $MnSO_4 \cdot H_2O$, $NiSO_4 \cdot 6H_2O$, $(NH_4)_2Fe(SO_4)_2 \cdot 6_{H2}O$, $CoSO_4$ and $CuSO_4 \cdot 5H_2O$ in 5 mL of deionized water each. Then, 50 mL of a solution of 0.1 M $Na_2WO_4 \cdot 2H_2O$, and 11 mM of Na_2HPO_4 was vigorously stirred with a magnetic stirrer for 5 minutes. Concentrated acetic acid was then added to this solution to adjust it to a pH of 7. Finally, each solution of transition metal ions was added to 10 mL of tungstate solution, and the obtained mixtures were refluxed for two hours, followed by hot filtering. 0.4 g of KCl was added to the filtrate, and the solutions were left to crystalize overnight. The solutions were then filtered to obtain the crystals, which were then redispersed in deionized water and heated until dissolved. The following day, the recrystallized products were obtained by decanting the excess solution and being left to dry at room temperature. The resulting transition metal POMs were as follows: $K_6Na_4[X_4(H_2O)_2(PW_9O_{34})_2] \cdot 24H_2O$ where (X = Ni, Mn, Cu, Co, Fe).

To prepare the composites with different POM to rGO ratios, firstly the amounts of each component, previously ground, were weighed, and 1 mL of ethanol was added. The mixture was then sonicated for 2 h and then left to dry over 2 days.

Physico-chemical characterization of materials was done in collaboration with the Faculty of Physical Chemistry, University of Belgrade, Serbia. The synthesized POM/rGO composites were characterized in terms of their structure, present surface functional groups, surface morphology and atomic composition.

For the investigation of the structure of the five different POM/rGO materials, an X-ray diffraction (XRD) analysis was performed using a Rigaku Ultima IV diffractometer in Bragg-Brentano geometry, with Ni-filtered CuKα radiation (λ=1.54178 Å). Diffraction data was obtained using scattering angle 2 θ from 20 to 90° with a step of 0.020° and acquisition rate of 2° min^{-1}.

Fourier-transform infrared (FTIR) spectroscopy analysis was carried out using Perkin Elmer GX1 spectrometer to determine the surface functional groups of the POMs/rGO samples.

Examination of surface morphology and determination of atomic composition was made by Phenom™ ProX Desktop (Thermo Fisher Scientific™, Waltham, MA, USA) scanning electron microscope with integrated energy-dispersive X-ray spectroscopy (SEM-EDX) detector.

Electrocatalysis using POM/rGO composites

To discern which of the prepared POM/rGO materials is the best as electrocatalyst for OER and ORR, a single cell was built, with a saturated calomel electrode (SCE) as reference, a platinum coil as counter electrode, and as working electrode a POM/rGO material in the form of a thin film on a glassy carbon rod substrate. All electrodes were placed in 80 mL of 1 M KOH, which was used as the supporting electrolyte. The measurements were done using a Squidstat™ potentiostat from Admiral Instruments.

Two sets of studies were done: first set with composites of polyoxometalates coordinated with different transition metals and reduced graphene oxide (rGO), all at a 5:1 ratio of POMs to rGO, and second set for the best POM/rGO with different POM to rGO ratios (1:5, 2:4, 3:3, 4:2, 5:1) as well as with pure rGO and pure POM. Additionally, one sample of 1:5 ratio of POM to activated carbon (AC) was prepared.
Catalytic inks were all prepared in the same manner: 6 mg of POM/rGO composites, all at a ratio of 5:1 POM to rGO, were weighted into glass vials, and then 600 µL of deionized water, 400 µL of 96% ethanol, and 25 µL of 0.5 wt.% Nafion™ in ethanolwere added. To ensure homogeneity, the inks were all sonicated for 30 minutes in an Emmi® - 08ST sonicator from EMAG Technologies®. To prepare the inks with different POM to rGO ratios, firstly the amounts of each component, previously ground, were weighed, and 1 mL of ethanol was added, The mixture was then sonicated for 2 hours, and finally it was left to dry for 2 days.

The inks were then pipetted onto the glassy carbon rod with total area of 0.5 cm^2, leading to a loading of 0.176 mg cm^{-2} of catalyst.

Then capacitance measurements were done, all in N_2 saturated solution, achieved by bubbling the electrolyte solution in N_2 for 15 minutes before the experiments and, at a lower flow while running them. After these measurements, O_2 is bubbled in the solution for 5 minutes to remove N_2, at which point OER LSVs were run, 5 for each material. Finally, electrochemical impedance spectroscopy (EIS) was carried out in the frequency range from 100 kHz to 0.1 Hz at several different potentials (1.57, 1.67, and 1.77 V).

The activity of five POM/rGO composites was also examined for HER as cathodic reaction in water electrolysis process, the main process for production of green hydrogen. However, the composites showed no activity for HER.

To study the ORR the samples were tested using cyclic voltammetry with a rotating disk electrode. The same three-electrode electrochemical system was used. 20 µl of ink was applied to the rotating disk electrode. The rotational speed of the disc electrode was varied for each CV, with the rotation speeds being the following: 300, 600, 900, 1200, 1800, 2400, and 3600 rpm. The range of potentials swept was from -0.8 V to 0 V vs. SCE, at a scan rate of 5 mV s^{-1}. iR correction was included during the measurement, performed by a Ivium V01107 Potentiostat/Galvanostat from Ivium Technologies.

Finally, a series of experiments were devised to discover which of our POMs is best as a catalyst for metal/air batteries. Firstly, the best metal to use as anode needed to be discovered, so a preliminary cell setup was used, with carbon paper as the current collector on the cathodic side, 1M KOH as electrolyte, and a piece of paper towel as the separator. With this configuration, a few metals were tested, with the selection factor being which had higher open circuit potential.

With this criteria, it was determined that the best metal was aluminium plate. With this information combined with other optimization parameters from [55], the final design used was a follows: aluminium plate anode, 4 M KOH electrolyte, cotton pad separator and carbon paper cathodic current collector. With it we tested each POM, with rGO at a ratio of 5:1. The loading of catalytic ink, prepared in the same manner as for the fundamental electrochemical studies, was 800 µL per piece of carbon paper, leading to loadings between 1.73 and 3.55 mg cm^{-2} as is summarised in the next table (Table 3.1).

Table 3.1: Loadings of POM/rGO composites on the cathode in a metal-air battery setup.

Ink	POM/rGO(mg cm^{-2})
Ni-POM/rGO	2.32
Co-POM/rGO	3.55
Mn-POM/rGO	1.73
Fe-POM/rGO	2.32
Cu-POM/rGO	2.17

Then, using the metal-air battery setup employing the best POM/rGO as the cathode catalyst, the electrolyte composition was optimised. Thereafter, new power density curves were recorded for batteries with Co-POM/rGO as cathode catalyst, but with KOH electrolyte concentrations of 0.5; 1; 2 and 4 M. At 6 M KOH and beyond, the reaction of Al with OH^- became too violent, boiling the electrolyte immediately, causing this attempt, and others at even higher concentrations to be discarded.

Part III

Results and Discussion

Characterisation of the synthesized transition metal POMs/rGO composites

XRD diffractograms of all studied electrocatalysts are presented in Fig. 3.7A. All of the five samples show a broad peak at 2θ of 25° corresponding to the reflections from the rGO crystal planes. Characteristic peaks of POMs structure are not observed because of the highly dispersed state of POMs on the surface of rGO in the synthesized POMs/rGO materials [66, 67, 68, 69].

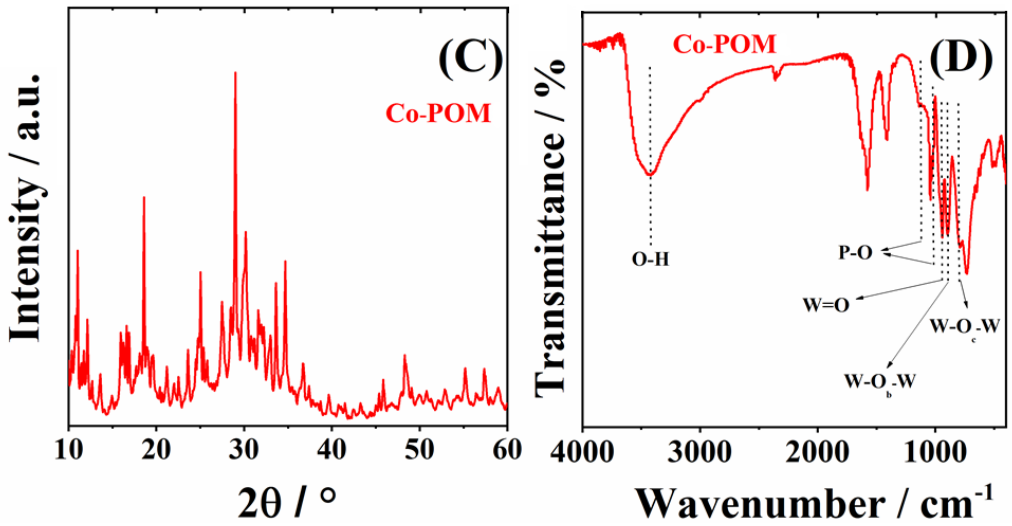

Figure 3.6: XRD diffractograms (A), and FTIR spectra (B) of pure Co-POM.

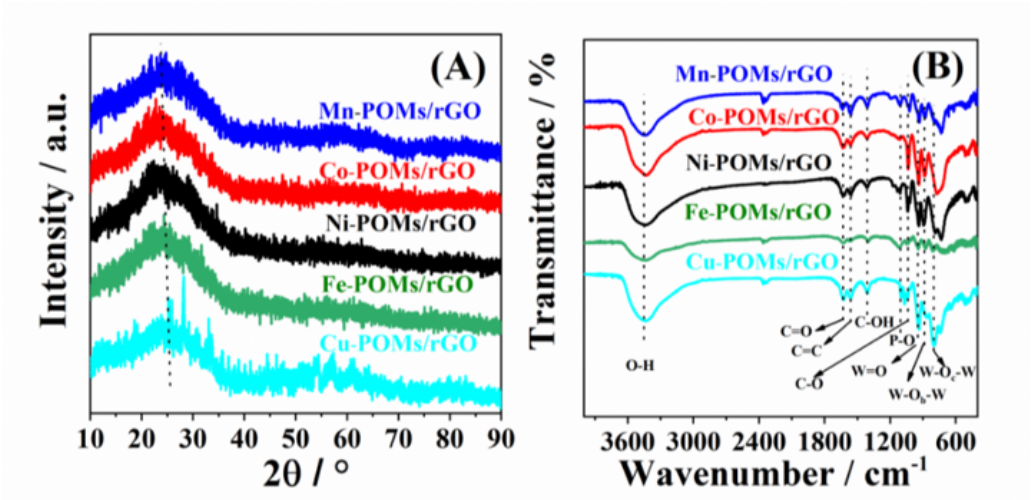

Figure 3.7: XRD diffractograms (A), and FTIR spectra (B) of Ni-POM/rGO, Co-POM/rGO, Mn-POM/rGO, Fe-POM/rGO, and Cu-POM/rGO electrocatalysts.

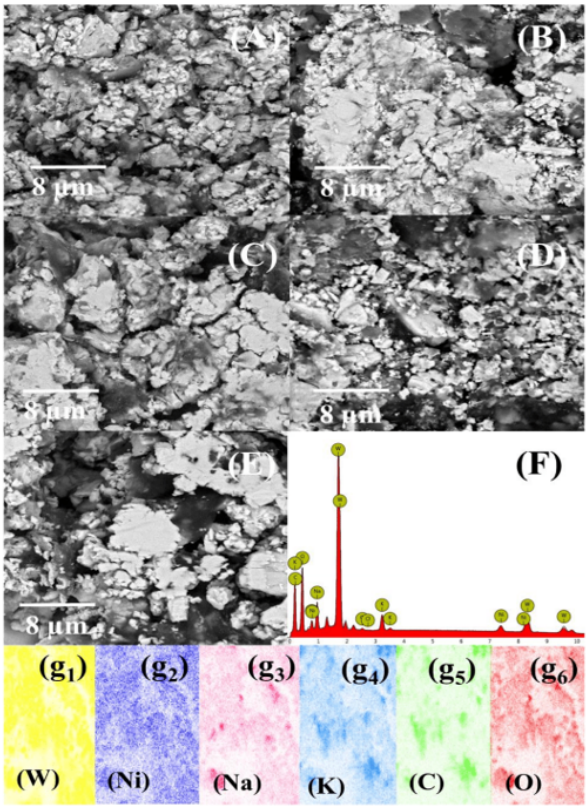

Figure 3.8: SEM images of Co-POM/rGO (A), Cu-POM/rGO (B), Fe-POM/rGO (C), Mn-POM/rGO (D), and Ni-POM/rGO (E), with EDS spectrum (F), and the elemental mapping of Ni-POM/rGO (g1-g6).

FTIR spectra of POM/rGO composites reveal the four characteristic POMs bands at 1108, 947, 881, and 802 cm^{-1}, Fig. 3.7B corresponding to the frequency of P-O in the central PO_4, W=O in the exterior WO_6, $W - O_b - W$, and $W - O_c - W$ bridges, respectively [67, 69, 70]. Absorption rGO bands, fig. 3.7B, were observed at 1683, 1561, 1402, and 1038 cm^{-1} and could be associated with C=O, C=C, C-OH, and C-O, respectively [67, 71]. The low intensity of rGO bands compared with the intensity of the graphene oxide (GO) absorption band is a consequence of the reduction of oxygen functionalities in rGO [67]. The FTIR spectra of POMs/rGO composite confirmed that the structures of POMs and rGO are preserved in all five samples.

SEM images of the POM/rGO composites, Fig. 3.8A-E, clearly show uniform morphology of all five samples. The typical layered morphology of rGO was observed with POMs nanoparticles anchored to rGO sheets [67, 66, 71]. The presence of metal (Ni, Co, Mn, Cu, or Fe) within the corresponding POM/rGO composite structure was confirmed by SEM-EDS analysis, Fig. 3.8F illustrates the case of Ni- POM/rGO. Furthermore, elemental mapping revealed uniform distribution of metal in the corresponding composite as well as of elements originating from the POMs/rGO structure (W, Na, K, C, and O), Fig. 3.8 again illustrates the case of Ni- POM/rGO.

Study of POM/rGO composites as electrocatalysts for OER

LSVs of five studied POM/rGO (5:1) composites were first recorded under OER polarization conditions in 1 M KOH to evaluate their potential as electrocatalysts for OER, Fig. 3.9. The LSVs immediately reveal the highest current density in case of Ni-POM/rGO and negligible current density in case of Cu-POM/rGO within the studied potential range. Onset potential (E_{onset}), defined as the potential to reach a current density of 1 mA cm^{-2}, was found to increase in the order Ni-POM/rGO (1.553 V) < Co-POM/rGO (1.605 V) < Fe-POM/rGO (1.615 V) < Mn-POM/rGO (1.656 V). Furthermore, the current density at an overpotential (difference between the measured potential and the equilibrium potential of 1.24 V) of 400 mV (j_{400}) was found to decrease in the order Ni-POM/rGO (21.822 mA cm^{-2}) > Co-POM/rGO (3.074 mA cm^{-2}) > Fe-POM/rGO (1.726 mA cm^{-2}) > Mn-POM/rGO (0.450 mA cm^{-2}) > Cu-POM/rGO (0.199 mA cm^{-2}). Thus, Mn-POM/rGO and Cu-POM/rGO did not reach a current density of 10 mA cm^{-2} within the studied potential range. Ni-POM/rGO exhibited the lowest overpotential to reach a current density of 10 mA cm^{-2} (η_{10}) of 0.366 V, which was approximately 54 mV and 85 mV lower than that of Co-POM/rGO (0.420 V) and Fe-POM/rGO (0.451 V), respectively. Next, Tafel analysis was performed to get further insight into the electrocatalysts properties and activity for electrocatalysis of OER. Therefore, LSVs recorded under the OER polarization conditions were used for the construction of potential (E) vs. the logarithm of current density (log j) plots. The slope of these plots, the so-called Tafel slope (b), reflects the rate of current density change with the increase in (over) potential. Ni-POM/rGO (0.068 V dec^{-1}), Co-POM/rGO (0.062 V dec^{-1}), and Mn-POM/rGO (0.066 V dec^{-1}) showed similar values of Tafel slope, while Tafel slope value of Fe-POM/rGO (0.074 V dec^{-1}) was somewhat higher.

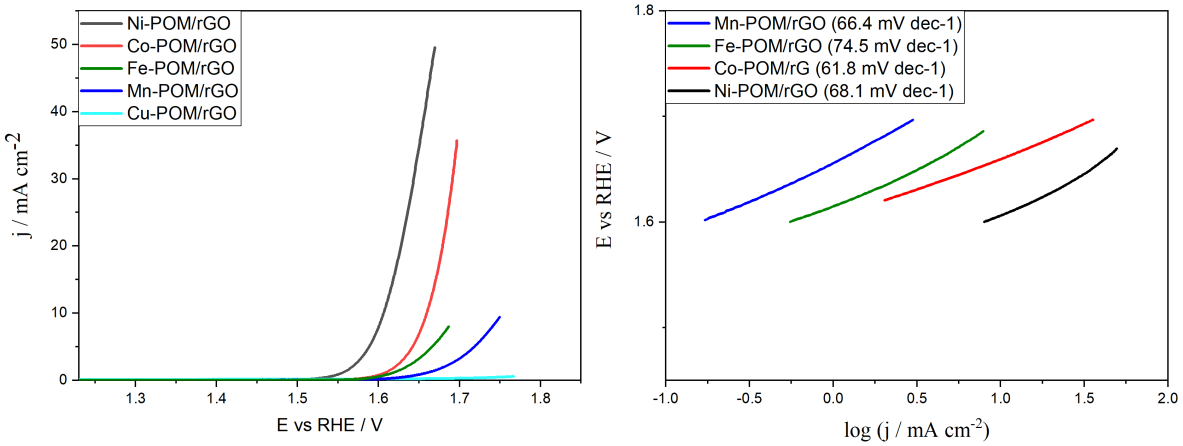

Figure 3.9: LSVs of five studied POM/rGO electrocatalysts in 1 M KOH (A) with the corresponding Tafel plots (B).

For LSV plotting, ohmic drop correction is first made to the measured potentials, accounting for electrolyte resistance by applying the formula given in the theoretical introduction.
Table 3.2 summarises the main reaction parameters for OER at studied POM/rGO composites.

Table 3.2: Kinetic parameters of OER for POM/rGO (5:1) electrocatalysts.

Catalyst	Tafel slope (mV dec^{-1})	E_{onset} (V vs. RHE)	η_{10} (mV)	j_{400} (mA cm^{-2})
Cu-POM/rGO	——	——	——	0.199
Mn-POM/rGO	66.4	1.656	——	0.450
Fe-POM/rGO	74.5	1.615	0.467	1.73
Co-POM/rGO	61.8	1.605	0.430	3.07
Ni-POM/rGO	68.1	1.553	0.376	21.8

Where —— for E_{onset} and η_{10} means that the values of 1 mA cm^{-2} and 10 mA cm^{-2} where not reached.

To discern the best catalyst for OER, several different factors need to be considered. Firstly, the lower Tafel slope, the better the electrocatalytic performance of a composite; still, Tafel slope values for Co-, Fe- and Ni-POM/rGO are quite similar. The difference appears then in the values of onset potential and current at an overpotential of 400 mV. As can be seen in table 3.2, Ni-POM/rGO presented the lowest onset potential. Similarly, at potential of 1.63 V vs. RHE (overpotential of 400 mV) the current density reached using Ni-POM/rGO was much higher compared to the other four composites. The significance of these values is clear in the LSV, where Ni clearly shows higher currents for almost all the potential range.

To gain insight into the POM/rGO electrical properties, electrochemical impedance measurements were carried out under OER polarization conditions. Electrolyte resistance (R_s) was similar in case of all studied composites with small variations resulting from small variations in the cell geometry and arrangement. Resistance to charge transfer at the electrode surface – electrolyte interface (R_{ct}), equivalent to the diameter of the semicircle in the Nyquist plots, was observed to be significantly different for the studied composites. Figure 3.10 depicts the Nyquist plots recorded at the potential of 1.57 V where Ni-POM/rGO exhibits the charge transfer resistance of only 21.5 Ω in comparison to 207 and 396 Ω in the case of Co-POM/rGO and Fe-POM/rGO, respectively. Decrease in charge transfer resistance with the increase of the potential could be seen for all studied composites (Fig. A.3). The lowest charge transfer resistance in the case of Ni-POM/rGO can account for the highest current densities recorder and its overall best performance for OER.

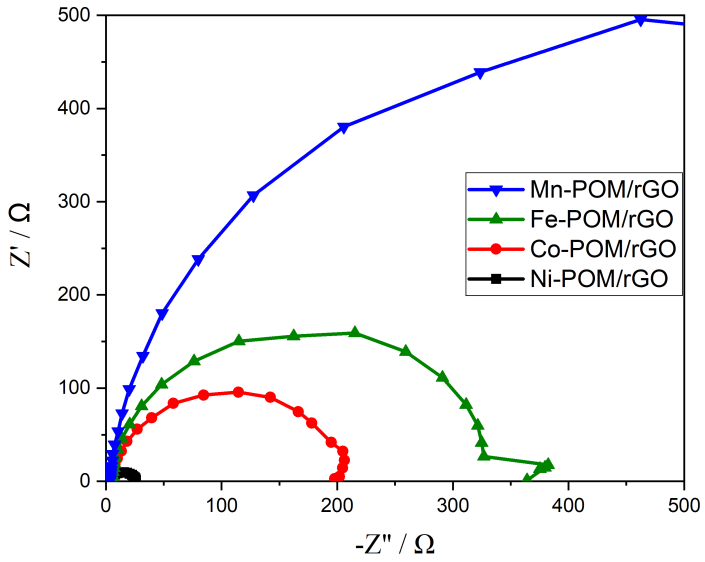

Figure 3.10: Nyquist plots of POM/rGO electrocatalysts at 1.57 V.

Furthermore, double-layer capacitance (C_{dl}) measurements were done in a non-faradaic region, Fig. A.1. Double-layer capacitance value is directly proportional to the material's electrochemically active surface area (ESCA) and thus to the number of active cites. Double-layer capacitance values for studied POM-rGO composites were found to range from 0.386 to 0.715 mF cm^{-2}. All composites show the values of double-layer capacitance of the same order indicating similar ECSA. It is important to note that the high-surface-area rGO contributes to the non-faradaic, capacitive currents and, consequently, affects ECSA determination. Still, the present estimation by the Cdl method is suitable for the ECSAs comparison, as all the studied materials contain rGO.

With all this data, it is easy to conclude that of all the POMs studied, Ni-POM/rGO is the best for OER. The capacitance values are explicit in the following table 3.3.

Table 3.3: Double-layer capacitance values of different POMs/rGO composites.

Catalyst	Double layer capacitance (mF cm^{-2})
Cu-POM/rGO	0.525
Mn-POM/rGO	0.386
Fe-POM/rGO	0.715
Co-POM/rGO	0.505
Ni-POM/rGO	0.362

To find the optimum composition of the POM/rGO nano-composites, i.e., the ratio of POM:rGO that would lead to the highest electrocatalytic activity, similar experiments were carried out for different ratios.

Study of Ni-POM/rGO with different POM:rGO ratios as electrocatalysts for OER

After determining that Ni-POM/rGO is the most active for OER, 5 different ratios of POM:rGO were studied, 1:5,2:4, 3:3, 4:2, 5:1, along with pure Ni-POM and pure rGO under the same conditions as the studies for different POMs. For comparison, IrO_2, a benchmark noble-metal based catalyst for OER was also studied.

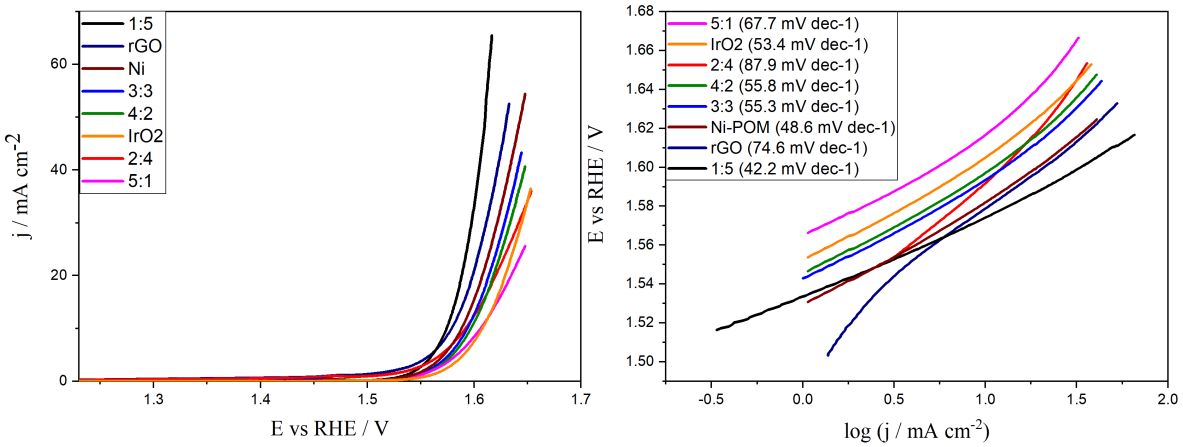

Figure 3.11: LSVs of Ni-POM/rGO in 1 M KOH with different POM:rGO ratios (A) with the corresponding Tafel plots (B).

The LSVs here presented are plotted, again, after ohmic drop correction.
Again, the LSVs immediately reveal the highest current density for a ratio of 1:5 Ni-POM:rGO. E_{onset}, was found to increase in the order rGO (1.46 V) < Ni-POM:rGO (2:4) (1.50 V) < Ni-POM:rGO (1:5) (1.53 V) < Ni-POM:rGO (3:3) (1.54 V)< Ni-POM (1.54 V) < Ni-POM:rGO (5:1) (1.55 V)< Ni-POM:rGO (4:2) (1.55 V)< IrO_2 (1.56 V). Furthermore, j_{400} was found to decrease in the order Ni-POM:rGO (1:5) (83.45 mA cm^{-2}) < Ni-POM (53.98 mA cm^{-2}) < rGO (49.43 mA cm^{-2}) < Ni-POM:rGO (3:3) (28.00 mA cm^{-2}) < Ni-POM:rGO (4:2) (27.62 mA cm^{-2}) < Ni-POM:rGO (2:4) (24.19 mA cm^{-2}) < IrO_2 (20.61 mA cm^{-2}) < Ni-POM:rGO (5:1) (14.96 mA cm^{-2}). rGO exhibited the lowest overpotential to reach a current density of 10 mA cm^{-2} (η_{10}) of 349 mV, which was just 5 mV and 6 mV lower than that of Ni-POM/rGO (1:5) and Ni-POM, respectively. Next, Tafel analysis was performed, leading to the Tafel slope values presented in table 3.4, where it can be seen that Ni-POM/rGO (1:5) has the lowest Tafel slope.

Table 3.4: Kinetic parameters of OER for different Ni-POM:rGO ratios and IrO_2 electrocatalysts.

Catalyst	Tafel slope (mV dec^{-1})	E_{onset} (V vs RHE)	η_{10} (mV)	j_{400} (mA cm^{-2})
Ni-POM	48.6	1.54	355	53.98
1:5	42.2	1.53	354	83.45
2:4	87.9	1.50	362	24.19
3:3	55.3	1.54	364	28.00
4:2	55.8	1.55	368	27.62
5:1	67.7	1.55	381	14.96
rGO	74.6	1.46	349	49.43
IrO_2	53.4	1.56	378	20.61

A table can also be done with materials reported in the literature to compare with the studied POMs (Table 3.5).

Table 3.5: Tafel slopes of POMs in the literature.

Material	Tafel slope (mV dec^{-1})	Reference
MWCNT_N8_Co4	55	[21]
GF_N8_Co4	67	[21]
GF_ND8_Co4	68	[21]
GF_NS8_Co4	62	[21]
Mono(aqua)nickel(II)	168	[26]
Ru_4POM	120	[72]
Co_4POM	80	[72]
Co6.8Ni1.2W12O42(OH)4(H2O)8/Ni Foam	126	[73]
NiP4Mo6	73	[40]
Fe2Ni2@MWCNT$_N$6	45	[44]
Fe4@MWCNT$_N$6	102	[44]
Ni4@MWCNT$_N$6	54	[44]
ZIF-8@ZIF-67@POM	88	[74]
Ba[Fe4-WS]/CP	99	[29]
Ba[Co4-WS]/CP	73	[29]
PBA@POM	235	[75]
1-CoW	53	[30]
2-CoFeW	43	[30]
3-CoFeW	38	[30]

Co4—$[Co_4(H_2O)_2(PW_9O_{34})_2]$; Mono(aqua)nickel(II)—$[Ni^{II}(2,2{-}bpy)_3]_3[Ni^{II}(2,2{-}bpy)_2(H_2O)HCo^{II}W_{12}^{VI}O_{40}]_2{\cdot}H_2O$; Ru4POM—$[Ru_4O_4(OH)_2(H_2O)_4(\gamma{-}SiW_{10}O_{36})_2]^{10-}$; Co4POM—$[Co_4(H_2O)_2(PW_9O_{34})_2]^{10-}$; NiP4Mo6—$Ni_3[Mo_6O_{12}(OH)_3(HPO_4)_3(PO_4)]_2{\cdot}4bpe{\cdot}10H_2O$, bpe = 4,4-vinylene-dipyridine; Fe2Ni2—$Na_{14}[(FeOH_2)_2Ni_2(As_2W_{15}O_{56})_2]{\cdot}55H_2O$; Fe4—$(Na_{12}[(FeOH_2)_2Fe_2(As_2W_{15}O_{56})_2]{\cdot}54H_2O$; Ni4—$Na_{12}[(NiOH_2)_2Ni_2(As_2W_{15}O_{56})_2]{\cdot}54H_2O$; ZIF-8@ZIF-67@POM—zeolitic imidazolate frameworks@$H_3[PW_{12}O_{40}]{\cdot}nH_2O$; Ba[Fe4-WS]—$[Fe_4^{III}(H_2O)_2(B{-}\alpha{-}PW_9O_{34})_2]^{6-}$ and Ba[Co4-WS]/CP—$[Co_4^{II}(H_2O)_2(B-\alpha-PW_9O_{34})_2]^{10-}$, with carbon paste (CP); POM in PBA@POM—$H_3PMo_{12}O_{40}$.

The main reaction parameters for OER are present in table 3.4. Firstly, the Tafel slope of Ni-POM/rGO (1:5) is clearly the lowest. The activity of this ratio can also be differentiated from the others by the high value of j_{400}, and low overpotential to reach 10 mA cm^{-2}.

By comparing the values obtained for the studied POMs/rGO with ones from the literature, it can be concluded that Ni-POM/rGO has a comparable Tafel slope to the best material found in other papers.

Electrochemical impedance measurements were carried out under OER polarization conditions. While again, R_s was similar in the case of all studied composites, high variations in R_{ct} can be observed in Figure 3.12, which depicts the Nyquist plots recorded at the potential of 1.57 V. Here Ni-POM/rGO (1:5) exhibits the lowest charge transfer resistance of only 10.0 Ω in comparison to 20.0 Ω in case of Ni-POM/rGO (4:2), Ni-POM/rGO (5:1) and rGO, respectively. Decrease of charge transfer resistance with the increase of the potential could be seen for all studied composites(Fig. A.4). The lowest charge transfer resistance in the case of Ni-POM/rGO (1:5) can account for the highest current densities recorder and its overall best performance for OER.
Furthermore, double-layer capacitance (C_{dl}) measurements were done in a non-faradaic region, Fig. A.2. Double-layer capacitance values for studied Ni-POM/rGO composites were found to range from 0.337 to 0.815 mF cm^{-2}.

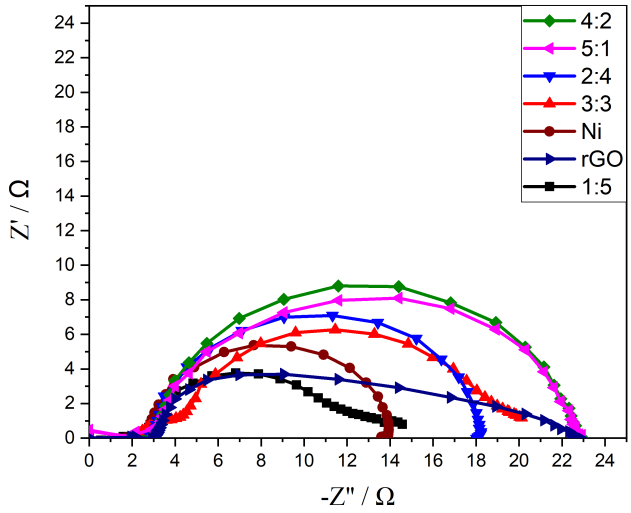

Figure 3.12: Impedance graph for different Ni-POM:rGO ratios at 1.57 V.

The study of impedance for these materials follows what is expected, catalysts with higher current density show lower resistance. From this data, it is easy to conclude that of all the POMs studied, and in comparison with the industry benchmark IrO_2, Ni-POM:rGO ratio of (1:5) is the best for OER.

Another observation is that all of the materials showed increased activity with each additional LSV run; this may be due to the fact that with each LSV, more Ni oxide is formed, which according to the literature [76] has higher activity for OER than metallic Ni, increasing the current with Ni oxide amount.

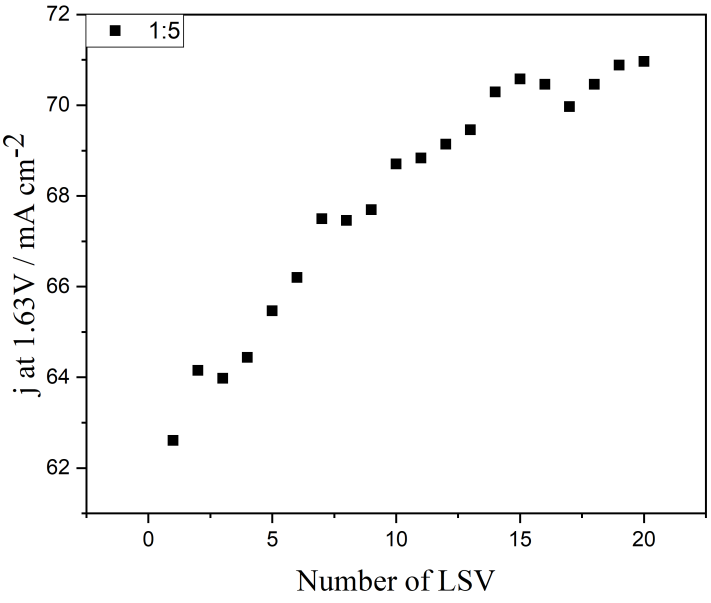

Figure 3.13: Current density recorded at 1.63 V using Ni-POM/rGO in 1 M KOH with sequential LSVs.

But another thing to consider is the catalyst price. By dividing material price per electrode loading, a table (table 3.6) can be drawn comparing the price of each catalyst per unit of area.

Table 3.6: Catalyst prices per unit of area.

Catalyst	Cheapest price ($\$ m^{-2}$)	Second cheapest price ($\$ m^{-2}$)	Sigma Aldrich price ($\$ m^{-2}$)
Pure rGO	0.264	2.29	1128
1:5	0.651	2.52	940
2:4	1.04	2.76	753
3:3	1.43	2.99	566
4:2	1.81	3.23	379
5:1	2.20	3.46	191
IrO_2	0.141	0.704	844

The prices were calculated based on three different price points obtained online [77, 78, 79, 80, 81, 82, 83, 84].

As we can see, even though Ni-POM/rGO has better performance than IrO_2, as the price of rGO is considerably higher than IrO_2, it ends up as more expensive. But another price table can be created by taking into account performance (Table 3.7).

Table 3.7: Material prices per unit of current.

Catalyst	Cheapest price ($¢A^{-1}$)	Second cheapest price ($¢A^{-1}$)	Sigma Aldrich price ($¢A^{-1}$)
Pure rGO	0.0534	0.463	228
1:5	0.0780	0.302	113
2:4	0.429	1.14	311
3:3	0.509	1.07	202
4:2	0.656	1.17	137
5:1	1.47	2.31	128
IrO_2	0.0683	0.342	410

By including in the calculations, the current at an overpotential of 400 mV, it can be seen that the Ni-POM/rGO, at a ratio of 1:5 is always cheaper per unit of current produced than its noble metal counterpart. It is also very important to note that both the rGO and POMs studied in this thesis were synthesized in the in the university of Belgrade as a part of a joint project, meaning that both costs are substantially lower than for their commercial counterparts. As the synthesis process is relatively simple and uses cheap sustainable reagents, its scale-up to industrial level would not be a complicated process. From all this it is concluded that, the Ni-POM/rGO studied here outperforms for OER in every way current benchmark IrO_2 electrocatalyst in every way for OER.

Study of POM/rGO composites as electrocatalysts for ORR

To investigate potential use of POM/rGO composites as bifunctional electrocatalysts for oxygen electrode in metal-air batteries, i.e., for both OER and ORR, performance of POM/rGO composites was evaluated under ORR polarization conditions. ORR study was done using Ni-POM/rGO (1:5) and Co-POM/RGO (1:5) as the best and second-best electrocatalysts for OER among the five tested composites. To confirm materials' activity for ORR, two CVs are recorded for each material, in N_2- and O_2-saturated solution, Figure 3.14. Comparison of the recorded current densities shows clear increase in the presence of O_2 in case of both composites originating in the reduction of oxygen. Furthermore, it is evident that Co-POM/rGO (1:5) exhibits higher performance under ORR polarization conditions than Ni-POM/rGO (1:5) with current densities recorded using Co-POM/rGO being double those recorded using Ni-POM/rGO.

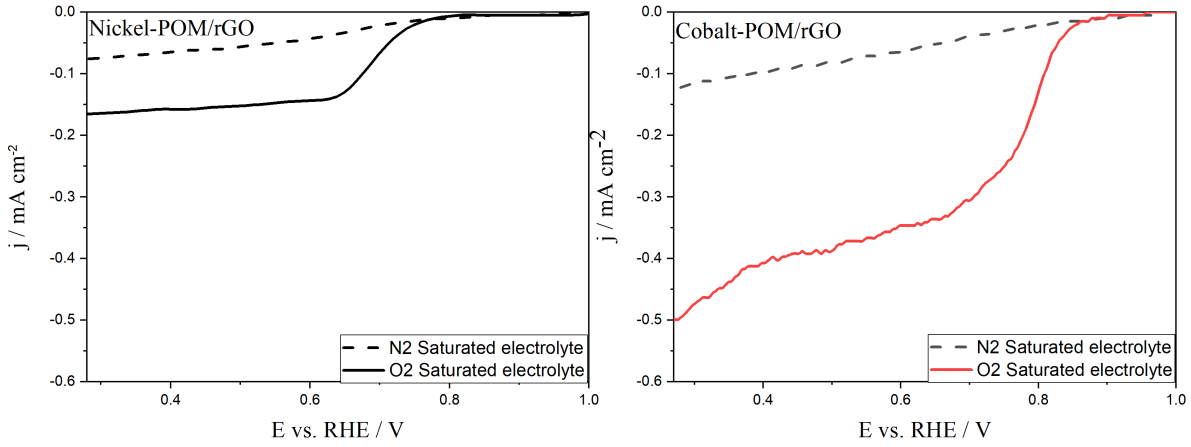

Figure 3.14: Cathodic scan of CVs of (A) Co-POM/rGO (1:5) and (B) Ni-POM/rGO (1:5) in N_2- and O_2-saturated 1 M KOH.

Subsequently, CVs were recorded using different electrode rotation rates, Figure 3.15. Onset potential (E_{onset}) as a measure of the electrocatalyst's activity, can be determined using different approaches in case of ORR. E_{onset} can be determined as the potential at which the recorded current density clearly deviates from the background current density. It can also be determined as the intersection point of the tangents to the baseline and to the rising current density part of CV. Finally, E_{onset}, can be defined as potential at the current density of -3 µA cm^{-2}. The onset potentials of two investigated electrocatalysts were determined (from CV curves at 1600 rpm) to be 0.767 and 0.719 V for Co-POM/rGO and Ni-POM/rGO respectively. Thus, Co-POM/rGO (1:5) showed more positive onset potential compared to Ni-POM/rGO (1:5) indicating its higher activity for ORR. Additionally, half-wave potential ($E_{1/2}$), as another widely-used indicator for the evaluation of the electrocatalytic activity of new electrode materials, was found to have a more positive value for Co-POM/rGO (1:5) (0.677 V) compared to Ni-POM/rGO (1:5) (0.620 V). Koutecký-Levich analysis was next performed at 3 different potentials. Number of electrons (n) transferred during ORR was determined from the slope of Koutecky-Levich plots (j^{-1} vs. $w^{-1/2}$), Figure 3.14. ORR n values for Co-POM/rGO (1:5) were found to range from 2.6 to 2.7 suggesting that reduction of oxygen proceeds by both 2-electron pathway (with production of HO_2^- as an intermediate) and 4-electron pathway (O_2

directly reduced to OH^-). 4-electron pathway is favourable mechanism for ORR in electrochemical energy conversion devices. On the other hand, n value for Ni-POM/rGO (1:5) was evaluated to range from 1.7 to 1.8 indicating a two-electron mechanism.

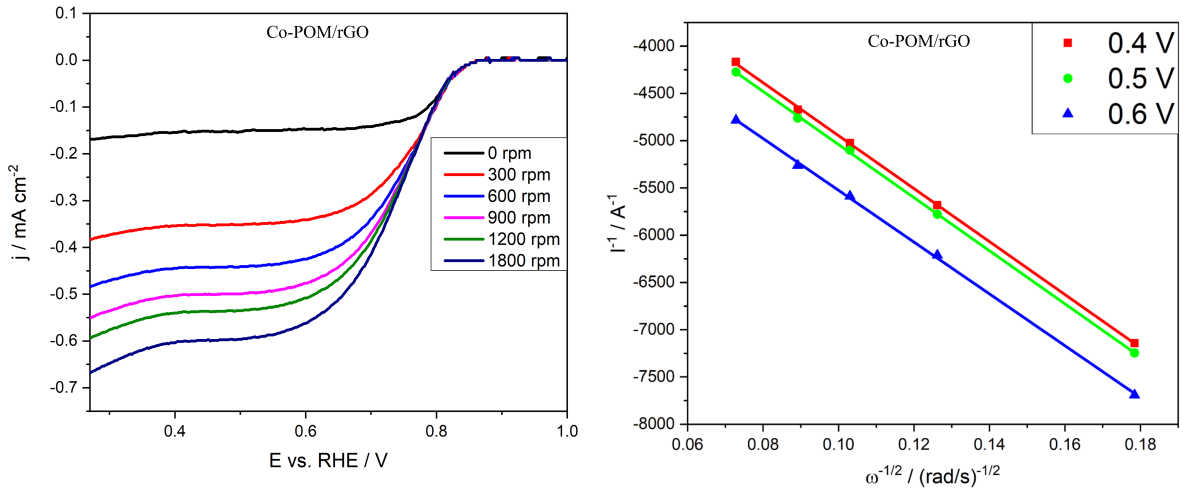

Figure 3.15: LSVs for Co-POM/rGO at different electrode rotation rates with the corresponding Koutecky-Levich analysis at three different potentials.

For ORR Tafel analysis was also done, similarly to OER, a lower absolute value of Tafel slope means higher activity for the reaction. Even though though these values for both POM/rGO composites are close, Co-POM/rGO has a lower Tafel slope of -165 mV dec^{-1}, compared with -175 mV dec^{-1} for Ni-POM/rGO.

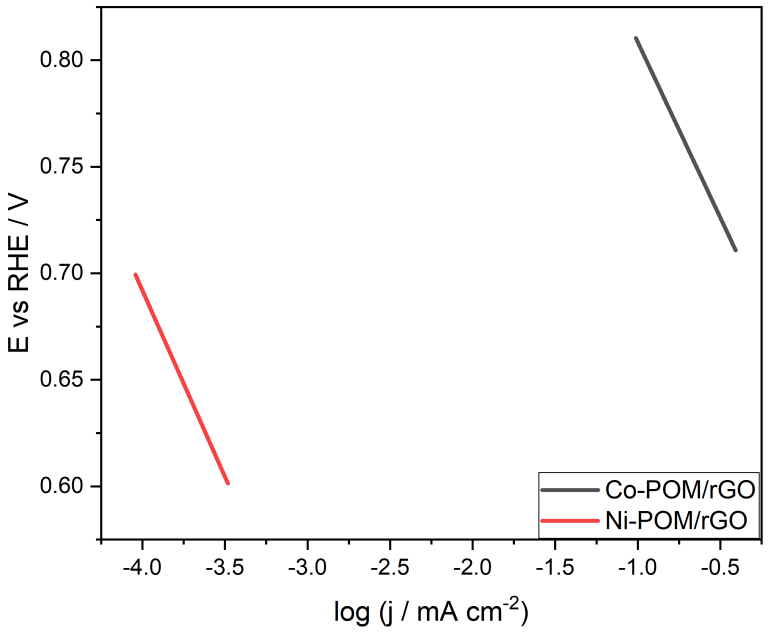

Figure 3.16: Tafel plots of the Co-POM/rGO (1:5) and Ni-POM/rGO (1:5) for ORR.

Table 3.8 summarizes the determined kinetic parameters of ORR at Co-POM/rGO (1:5) and Ni-

POM/rGO (1:5). More positive onset and half-wave potentials, slightly lower Tafel slope and higher number of electrons exchanged clearly demonstrate the superior performance of Co-POM/rGO for ORR compared to Ni-POM/rGO.

Table 3.8: Kinetic parameters of ORR at Co-POM/rGO (1:5) and Ni-POM/rGO (1:5).

Catalyst	Tafel slope (mV dec^{-1})	Number of exchanged electrons	Diffusion current density (mA cm^{-2})	Onset potential (V)	$E_{1/2}$ (V)
Co-POM/rGO	-165	2.6-2.7	1.07	0.826	0.711
Ni-POM/rGO	-175	1.7-1.8	0.82	0.719	0.620

Study of POM/rGO composites in a metal-air battery (MAB) setup

The last set of experiments carried out were the construction and study of metal-air batteries. Firstly, the optimum metal to use as anode needed to be determined, so a preliminary cell setup was used, with carbon paper as the current collector on the cathodic side, 1 M KOH as the electrolyte, and a piece of paper towel as a separator. With this configuration, a few metals were tested, with the selection factor being the cell's open circuit potential. And aluminum was found to be the optimum one.
Using the set-up already described, with Al plate, cotton separator, KOH electrolyte and catalyst deposited on carbon paper, firstly, the OCPs of all POMs were obtained with the use of a UNI-T 0T70B multi-metre, and they were, in ascending order, Ni-POM/rGO (1.386 V) < Co-POM/rGO (1.395 V) < Fe-POM/rGO (1.396 V) < Mn-POM/rGO (1.448 V) < Cu-POM/rGO (1.529 V). Then, all the materials were studied for the discharge of the battery leading to the following power density curves.

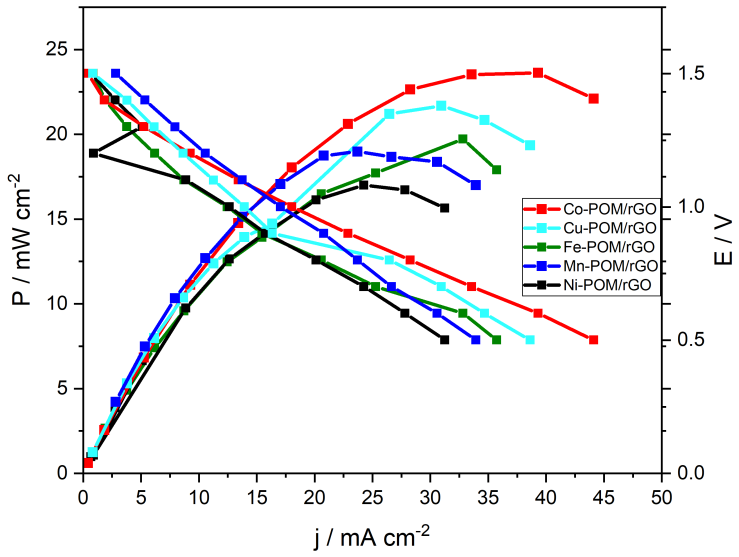

Figure 3.17: Power density curves of MAB with different POM/rGO composites as cathode electrocatalyst.

The maximum power densities obtained were, in ascending order, Ni-POM/rGO (17.0 mW cm^{-2}) < Mn-POM/rGO (19.0 mW cm^{-2}) < Fe-POM/rGO (19.7 mW cm^{-2}) < Cu-POM/rGO (21.7 mW cm^{-2}) < Co-POM/rGO (23.6 mW cm^{-2}).

As can be seen, and as was expected, the MAB with Co-POM/rGO has the highest energy density value. This is expected because the main reaction involved in metal-air battery discharge is ORR for which Co-POM/rGO exhibited highest activity.

One final study was carried out in the metal-air batteries, for the best material, several electrolyte concentrations were studied to enhance battery performance. As a final result, it can be observed that 4 M KOH was indeed the concentration for which the best results were reached.

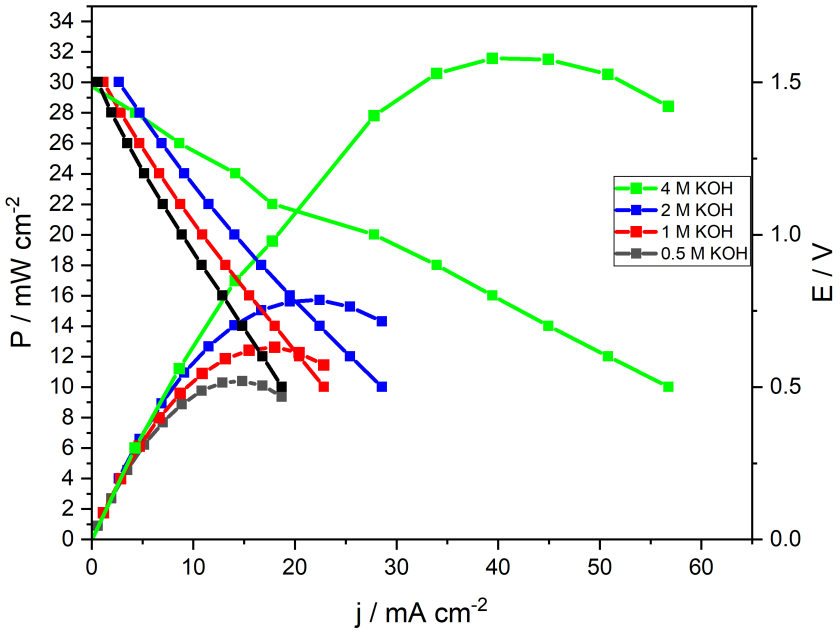

Figure 3.18: Power density curves of MAB with Co-POM/rGO cathode electrocatalyst and with KOH electrolyte of different concentrations.

Here, the maximum power densities obtained were, in ascending order, 0.5 M KOH (10.4 mW cm^{-2}) < 1 M KOH (12.6 mW cm^{-2}) < 2 M KOH (15.7 mW cm^{-2}) < 4 M KOH (31.6 mW cm^{-2}).

Co-POM/rGO prepred and studied whitin this Master thesis has shown excellent ORR and good OER activity that resulted in good performance of a metal-air battery employing it as electrode catalyst. The results show that it would be worth further optimization of a MAB utilizing this catalyst.

Part IV

Conclusions

POMs are a unique class of materials that have been shown to be suitable for improving performance on a variety of processes, following different approaches, from the very simple addition of POMs to activated carbon paste electrodes to more complex methods of chemical linking to emerging nanomaterials. As discussed, using POMs in batteries and supercapacitors (SCs) can enhance energy density by efficiently contributing to pseudocapacitive charge storage effects from their high surface-to-bulk ratio and multiple redox states. POMs are cheaper and easier to obtain in larger quantities than the noble metals based electrocatalysts which are currently the most active ones for the mentioned devices. Hence, their application holds the promise of contributing to overcoming the challenges of upgrading modern energy systems into more sustainable ones.

It is critical to develop new POM-based composites, particularly because of their poor electrical conductivity and high solubility in battery electrolytes, which results in low cycling stability and poor rate performance. Linking POMs to an appropriate conducting scaffold remains thus both fundamental and problematic. Particular attention should be given to POMs when used as electrode materials linked to carbon nanostructures that can potentially increase the conductivity of POMs. The energy storage mechanism for POMs-based electrode materials for rechargeable batteries and SCs is still not fully understood; the higher number of electron exchanges per molecule, when compared to other redox materials used in battery storage, makes it more complex to grasp. In the future, more in depth analysis will be necessary to understand the reactions at the electrode/electrolyte interface.

In this study, XRD, FTIR, and SEM-EDS techniques were used for the analysis of the structure and morphology of five different POMs/rGO electrocatalysts. SEM-EDS results showed the presence of five different metals (Ni, Co, Mn, Cu, and Fe) inside the POMs/rGO samples. FTIR spectra of NiPOMs/rGO, Co-POMs/rGO, Mn-POMs/rGO, Fe-POMs/rGO, and Cu-POMs/rGO electrocatalysts displayed characteristic bands for POMs and rGO structures.

And with the study of the conjugations of POMs and carbon structures, we could see that rGO addition significantly increased the currents for all reactions. For OER, Ni-POM/rGO was clearly the superior candidate, and further studies showed that the optimal Ni-POM:rGO ratio was 1:5. The current density values obtained with this catalyst were very promising, being even higher than that of IrO_2, the catalyst currently considered the best for this reaction. It is also important to note that even though Co-POM/rGO was not as good as Ni-POM, it came second best for OER.

In terms of ORR, Co-POM/rGO was the best; this, conjugated with the results from the MAB testing, lead us to conclude that Co-POM/rGO has very interesting as a bifunctional electrocatalyst for rechargeable metal-air batteries. Even though more in-depth studies of metal-air battery construction were not covered in the scope of this project, it would be interesting to analyse the results with the change of different parameters, namely separator composition, metal plate used, and even different carbon supports for the catalyst.

Part V

Bibliography and Annexes

Bibliography

[1] URL: https://gadebate.un.org/en/77/secretary-general-united-nations (visited on 01/10/2022).

[2] U. Ghosh et al. “Review – Hydrocracking using different catalysts”. In: *Chem. Process Eng. Res.* 34 (2015), pp. 51–56.

[3] H. Wang et al. “Molecular cluster batteries of nano-hybrid materials between Keggin POMs and SWNTs”. In: *Dalt. Trans.* 41 (2012), pp. 9863–9866. DOI: 10.1039/c2dt30603d.

[4] H. Wang et al. “In operando X-ray absorption fine structure studies of polyoxometalate molecular cluster batteries: Polyoxometalates as electron sponges”. In: *J. Am. Chem. Soc.* 134 (2012), pp. 4918–4924. DOI: 10.1021/ja2117206.

[5] J. Chen et al. “Metal hydride mediated water splitting: Electrical energy saving and decoupled H2/O2 generation”. In: *Mater.Today* 47 (2021), pp. 16–24. DOI: 10.1016/j.mattod.2021.02.019.

[6] S.A. Grigoriev et al. “Current status, research trends, and challenges in water electrolysis science and technology”. In: *Int. J. Hydrogen Energy* 45 (2020), pp. 26036–26058. DOI: 10.1016/j.mattod.2021.02.019.

[7] N. Kawasaki et al. “Nanohybridization of polyoxometalate clusters and single-wall carbon nanotubes: Applications in molecular cluster batteries”. In: *Angew. Chemie - Int. Ed.* 50 (2011), pp. 3471–3474. DOI: 10.1002/anie.201007264.

[8] X. López, J.A. Fernández, and J.M. Poblet. “Redox properties of polyoxometalates: New insights on the anion charge effect”. In: *J. Chem. Soc. Dalt. Trans.* 6 (2005), pp. 1162–1167. DOI: 10.1039/b507599h.

[9] X. López, C. Bo, and J.M. Poblet. “Electronic properties of polyoxometalates: Electron and proton affinity of mixed-addenda Keggin and wells-dawson anions.” In: *J. Am. Chem. Soc.* 124 (2002), pp. 12574–12582. DOI: 10.1021/ja020407z.

[10] A.E. Stamate et al. “Highlights on the catalytic properties of polyoxometalate-intercalated layered double hydroxides: A review”. In: *Catalysts* 10.57 (2020). DOI: https://doi.org/10.3390/catal10010057.

[11] URL: https://www.hioki.com/global/learning/electricity/nyquist.html#:~:text=A%5C%20Nyquist%5C%20plot%5C%20is%5C%20a,the%5C%20resistance%5C%20and%5C%20reactance%5C%20components. (visited on 04/10/2022).

[12] X.L. Wang et al. “A Series of polyoxometalate-based metal-bis(pyridyl-tetrazole) complexes with high electrocatalytic activity for hydrogen evolution reaction in alkaline and acid media”. In: *ACS Sustain. Chem. Eng.* 8 (2020), pp. 15696–15702. DOI: 10.1021/acssuschemeng.0c05459.

[13] Z. Yan et al. “Electrodeposition of (hydro)oxides for an oxygen evolution electrode.” In: *Chem. Sci.* 11 (2020), pp. 10614–10625. DOI: 10.1039/D0SC01532F.

[14] Y.V. Geletii et al. “An all-inorganic, stable, and highly active tetraruthenium homogeneous catalyst for water oxidation”. In: *Chemie., Int. Ed.* 47 (2008), pp. 3896–3899. DOI: 10.1002/anie.200705652.

[15] A. Sartorel et al. “Polyoxo-metalate embedding of a tetraruthenium(IV)-oxo-core by template-directed metalation of [γ-SiW10O36]8-: A totally inorganic oxygen-evolving catalyst.” In: *J. Am. Chem. Soc.* 130 (2008), pp. 5006–5007. DOI: 10.1021/ja077837f.

[16] Y. V. Geletii et al. “Homogeneous light-driven water oxidation catalyzed by a tetraruthenium complex with all inorganic ligands.” In: *J. Am. Chem. Soc.* 131 (2009), pp. 7522–7523. DOI: 10.1021/ja901373m.

[17] C. Besson et al. “Cs9[(γ-PW10O36)2Ru4O5(OH)(H2O)4], a new all-inorganic, soluble catalyst for the efficient visible-light-driven oxidation of water”. In: *Chem. Commun.* 46 (2008), pp. 2784–2786. DOI: 10.1039/b926064a.

[18] S.X. Guo et al. “Graphene-supported [Ru4O4(OH)2(H2O)4(γ-SiW10O36)2]10- for highly efficient electrocatalytic water oxidation”. In: *Energy Environ. Sci.* 6 (2013), pp. 2654–2663. DOI: 10.1039/c3ee41892h.

[19] M. Quintana et al. “Knitting the catalytic pattern of artificial photosynthesis to a hybrid graphene nanotexture.” In: *ACS Nano* 7 (2013), pp. 811–817. DOI: 10.1021/nn305313q.

[20] *How the race for cobalt risks turning it from miracle metal to deadly chemical*. URL: https://www.theguardian.com/global-development/2019/dec/18/how-the-race-for-cobalt-risks-turning-it-from-miracle-metal-to-deadly-chemical.

[21] N. Limani et al. “Cobalt Phosphotungstate-based composites as bifunctional electrocatalysts for oxygen reactions”. In: *Catalysts* 12 (2022). DOI: 10.3390/catal12040357.

[22] I. Zaharieva et al. “Electrosynthesis, functional, and structural characterization of a water-oxidizing manganese oxide”. In: *Energy Environ. Sci.* 5 (2012), pp. 7081–7089. DOI: 10.1039/c2ee21191b.

[23] S. Goberna-Ferrón, J. Soriano-López, and J.R. Galán-Mascarós. “Activity and stability of the tetramanganese polyanion [Mn4(H2O)2(PW9O34)2]10- during electrocatalytic water oxidation”. In: *Inorganics* 3 (2015), pp. 332–340. DOI: 10.3390/inorganics3030332.

[24] Y. Wu et al. “Study on catalytic water oxidation properties of polynuclear manganese containing polyoxometalates”. In: *Catalysts* 12 (2022). DOI: 10.3390/catal12020160.

[25] G. Zhu et al. “A nickel containing polyoxometalate water oxidation catalyst”. In: *Dalt. Trans.* 41 (2012), pp. 13043–13049. DOI: 10.1039/c2dt30331k.

[26] C. Singh and S.K. Mukhopadhyay S.and Das. “Polyoxometalate-supported Bis(2,2 -bipyridine) mono(aqua)nickel(II) coordination complex: An efficient electrocatalyst for water oxidation”. In: *Inorg. Chem.* 57 (2018), pp. 6479–6490. DOI: 10.1021/acs.inorgchem.8b00541.

[27] L. Yu et al. “Homogeneous electrocatalytic water oxidation at neutral pH by a robust trinuclear copper(II)-substituted polyoxometalate”. In: *Chem. Commun.* 54 (2018), pp. 354–357. DOI: 10.1039/c7cc08301g.

[28] L. Yu et al. “Efficient visible light-driven water oxidation catalyzed by an all-inorganic copper-containing polyoxometalate”. In: *Chem. Commun.* 51 (2015), pp. 17443–17446. DOI: 10.1039/c5cc07119d.

[29] K. Azmani et al. “Understanding polyoxometalates as water oxidation catalysts through iron vs. cobalt reactivity”. In: *Chem. Sci.* 12 (2021), pp. 8755–8766. DOI: 10.1039/d1sc01016f.

[30] X.B. Han et al. “Ultrasmall abundant metal-based clusters as oxygen-evolving catalysts”. In: *J. Am. Chem. Soc.* 141 (2019), pp. 232–239. DOI: 10.1021/jacs.8b09076.

[31] P.K. Sahoo et al. “2D-Layered Non-Precious Electrocatalysts for Hydrogen Evolution Reaction: Fundamentals to Applications.” In: *Catalysts* 11 (2021), p. 689. DOI: https://doi.org/10.3390/catal11060689.

[32] C. Singh et al. “Devising a polyoxometalate-based functional material as an efficient electrocatalyst for the hydrogen evolution reaction”. In: *Inorg. Chem.* 60 (2021), pp. 10302–10314. DOI: 10.1021/acs.inorgchem.1c00734.

[33] J.P. Cao et al. “First mononuclear copper(II) electro-catalyst for catalyzing hydrogen evolution from acetic acid and water.” In: *Int. J. Hydrogen Energy* 39 (2014), pp. 13972–13978. DOI: 0.1016/j.ijhydene.2014.07.030.

[34] D. Xue, Q.X. Peng, and S.Z. Zhan. “Synthesis and electrochemical properties of a water soluble nickel(II) complex supported by N-phenylpyridin-2-ylmethanimine ligand”. In: *Inorg. Chem. Commun.* 82 (2017), pp. 11–15. DOI: 10.1016/j.inoche.2017.04.018.

[35] T. Fang et al. “Electrochemical-driven water reduction catalyzed by a water soluble cobalt(III) complex with Schiff base ligand”. In: *Electrochim. Acta* 178 (2015), pp. 368–373. DOI: 10.1016/j.ijhydene.2014.07.030.

[36] D.M. Fernandes et al. “Polyoxometalate-graphene electrocatalysts for the hydrogen evolution reaction”. In: *ChemElectroChem* 5 (2018), pp. 273–283. DOI: 10.1002/celc.201701210.

[37] Y. Yang et al. “O-coordinated W-Mo dual-atom catalyst for pH-universal electrocatalytic hydrogen evolution”. In: *Sci. Adv.* 6 (2020), eaba6586. DOI: 10.1126/sciadv.aba6586.

[38] J. Gautam et al. “Heterostructure of polyoxometalate/zinc-iron-oxide nanoplates as an outstanding bifunctional electrocatalyst for the hydrogen and oxygen evolution reaction”. In: *J. Colloid Interface Sci.* 618 (2022), pp. 419–430. DOI: 10.1016/j.jcis.2022.03.103.

[39] A.W. Adamson et al. “Photochemistry of transition-metal coordination compounds”. In: *Chem. Rev.* 68 (1968), pp. 541–585. DOI: 10.1021/cr60255a002.

[40] Y. Zheng et al. “Surface O2- regulation on POM electrocatalyst to achieve accurate 2e/4e-ORR control for H2O2 production and Zn-air battery assemble”. In: *Appl. Catal. B Environ.* 285 (2021), p. 119788. DOI: 10.1016/j.apcatb.2020.119788.

[41] S. Zhang et al. “High oxygen reduction reaction performances of cathode materials combining polyoxometalates, coordination complexes, and carboneous supports”. In: *ACS Appl. Mater. Interfaces* 9 (2017), pp. 38486–38498. DOI: 10.1021/acsami.7b10989.

[42] R. Liu et al. “Top-down synthesis of polyoxometalate-like sub-nanometer molybdenum-oxo clusters as high-performance electrocatalysts”. In: *Chem. Sci.* 11 (2020), pp. 1043–1051. DOI: 10.1039/c9sc05469c.

[43] R. Liu et al. “Top-down synthesis of pol-yoxometalate-like sub-nanometer molybdenum-oxo clusters as high-performance electrocatalysts.” In: *Chem. Sci. 2020* 11 (2021), pp. 1043–1051. DOI: 10.1039/c9sc05469c.

[44] I.S. Marques et al. “Synergetic effects of mixed-metal polyoxometalates@carbon-based composites as electrocatalysts for the oxygen reduction and the oxygen evolution reactions”. In: *Catalysts* 12 (2022), p. 440. DOI: 10.3390/catal12040440.

[45] C. Lee et al. “Tetraruthenium polyoxometalate as an atom-efficient bifunctional oxygen evolution reaction/oxygen reduction reaction catalyst and its application in seawater batteries”. In: *ACS Appl. Mater. Interfaces* 12 (2020), pp. 32689–32697. DOI: 10.1021/acsami.0c07225.

[46] M.R. Horn et al. “Polyoxometalates (POMs): From electroactive clusters to energy materials”. In: *Energy Environ. Sci.* 14 (2021), pp. 1652–1700. DOI: 10.1039/D0EE03407J.

[47] Y. Lyu et al. “Recent advances in high energy-density cathode materials for sodium-ion batteries”. In: *Sustain. Mater. Technol.* 21 (2019), e00098. DOI: 10.1016/j.susmat.2019.e00098.

[48] J. Liu et al. ““Electron/Ion Sponge”-like V-based polyoxometalate: Toward high-performance cathode for rechargeable sodium ion batteries”. In: *ACS Nano* 11 (2017), pp. 6911–6920. DOI: 10.1021/acsnano.7b02062.

[49] J.J. Chen et al. “Design and performance of rechargeable sodium ion batteries, and symmetrical Li-Ion batteries with supercapacitor-like power density based upon polyoxovanadates”. In: *Adv. Energy Mater.* 8 (2018), p. 1701021. DOI: 10.1002/aenm.201701021.

[50] S. Hartung et al. “Vanadium-based polyoxometalate as new material for sodium-ion battery anodes”. In: *J. Power Sources* 288 (2015), pp. 270–277. DOI: 10.1016/j.jpowsour.2015.04.009.

[51] C.C. Lin et al. “Mechanism of sodium ion storage in Na7[H2PV14O42] anode for sodium-ion batteries”. In: *Adv. Mater. Interfaces* 5 (2018), p. 1800491. DOI: 10.1002/admi.201800491.

[52] X.Z. Yuan et al. “A review of all-vanadium redox flow battery durability: Degradation mechanisms and mitigation strategies.” In: *Int. J. Energy Res.* 43 (2019), pp. 6599–6638. DOI: 10.1002/er.4607.

[53] A. Clemente and R. Costa-Castelló. “Redox flow batteries: A literature review oriented to automatic control.” In: *Energies* 13 (2020), p. 4514. DOI: 10.3390/en13174514.

[54] M. Ulaganathan et al. “Recent Advancements in all-vanadium redox flow batteries”. In: *Adv. Mater. Interfaces* 3 (2016), p. 1500309. DOI: 10.1002/admi.201500309.

[55] F. Pan and Q. Wang. “Redox species of redox flow batteries: A review”. In: *Molecules* 20 (2015), pp. 20499–20517. DOI: 10.3390/molecules201119711.

[56] X. Wei et al. “Materials and systems for organic redox flow batteries: Status and challenges”. In: *ACS Energy Lett.* 2 (2017), pp. 2187–2204. DOI: 10.1021/acsenergylett.7b00650.

[57] H.D. Pratt and T.M. Anderson. “Mixed addenda polyoxometalate “solutions” for stationary energy storage”. In: *Dalt. Trans.* 42 (2013), pp. 15650–15655. DOI: 10.1039/c3dt51653a.

[58] D.P. Dubal et al. “Hybrid graphene-polyoxometalates nanofluids as liquid electrodes for dual energy storage in novel flow cells”. In: *Chem. Rec.* 18 (2018), pp. 1076–1084. DOI: 10.1002/tcr.201700116.

[59] M. Horn et al. “Supercapacitors: A new source of power for electric cars?” In: *Econ. Anal. Policy* 61 (2019), pp. 93–103. DOI: 10.1016/j.eap.2018.08.003.

[60] Y. Zhao et al. “Rational selection of small aromatic molecules to functionalize graphene for enhancing capacitive energy storage”. In: *J. Mater. Chem. A* 6 (2018), pp. 7566–7572. DOI: 10.1039/c8ta00710a.

[61] M. Horn et al. “Graphene-based supercapacitor electrodes: Addressing challenges in mechanisms and materials”. In: *Curr. Opin. Green Sustain. Chem.* 17 (2019), pp. 42–48. DOI: 10.1016/j.cogsc.2019.03.004.

[62] H.Y. Chen et al. “A polyoxovanadate as an advanced electrode material for supercapacitors”. In: *ChemPhysChem* 15 (2014), pp. 2162–2169. DOI: 10.1002/cphc.201400091.

[63] S. Gupta, B. Aberg, and S. Carrizosa. “Functionalized graphene–polyoxometalate nanodots assembly as “organic–inorganic” hybrid supercapacitors and insights into electrode/electrolyte interfacial processes”. In: *C* 3.24 (2017). DOI: 10.3390/c3030024.

[64] M.J. Craig et al. “Universal scaling relations for the rational design of molecular water oxidation catalysts with near-zero overpotential.” In: *Nat. Commun* 10.1 (2019). DOI: 10.1038/s41467-019-12994-w.

[65] J. M. Clemente-Juan et al. “Increasing The Nuclearity of Magnetic Polyoxometalates. Syntheses, Structures, and Magnetic Properties of Salts of the Heteropoly Complexes $[Ni_3(H_2O)_3(PW_{10}O_{39})H_2O]^{7-}$, $[Ni_4(H_2O)_2(PW_9O_{34})_2]^{10-}$, and $[Ni_9(OH)_3(H_2O)_6(HPO_4)_2(PW_9O_{34})_3]^{16-}$”. In: *Inorg.Chem.* 1.38 (1999), pp. 55–63. DOI: https://doi.org/10.1021/ic9807902.

[66] A. Ucar et al. “Catalytic degradation of organicdye using reduced graphene oxide–polyoxometalate nanocomposite”. In: *Materials Chemistry and Physics* 196 (2017), pp. 21–28. DOI: 10.1016/j.matchemphys.2017.04.047.

[67] F. Dehghani Sanij et al. “Fabrication of polyoxometalate-modified palladium-nickel/reduced graphene oxide alloy catalysts fo renhanced oxygen reduction reaction activity”. In: *RSC Advances* 11 (2021), pp. 39118–39129. DOI: 10.1039/d1ra06936e.

[68] N. Ross and N. Civilized Nqakala. “Electrochemical Determination of Hydrogen Peroxide by aNonenzymatic Catalytically Enhanced Silver-Iron (III) Oxide/Polyoxometalate/ReducedGraphene Oxide Modified Glassy Carbon Electrode”. In: *Analytical Letters* 53 (2020), pp. 2445–2464. DOI: 10.1080/00032719.2020.1745223.

[69] A. Khodadadi Dizaji, H.R. Mortaheb, and B. Mokhtarani. “Preparation of supported catalyst byadsorption of polyoxometalate on graphene oxide/reduced graphene oxide”. In: *Materials Chemistry and Physics* 199 (2017), pp. 424–434. DOI: 10.1016/j.matchemphys.2017.07.016.

[70] A. Tarlani et al. “Immobilization of Keggin and Preyssler tungsten heteropolyacids on various functionalized silica”. In: *Journal of Colloid and Interface Science* 303 (2006), pp. 32–38. DOI: 10.1016/j.jcis.2006.07.024.

[71] M.L. Yola et al. “Sensitive and selective determination of aqueous triclosan based on gold nanoparticles on polyoxometalate/reduced graphene oxide nanohybrid”. In: *RSC Advances* 5 (2015), pp. 65953–65962. DOI: 10.1039/c5ra07443f.

[72] Qiushi Yin et al. “Tafel Slope Analyses for Homogeneous Catalytic Reactions”. In: *Catalysts* 11.1 (2021). ISSN: 2073-4344. DOI: 10.3390/catal11010087. URL: https://www.mdpi.com/2073-4344/11/1/87.

[73] A Joshi. “A rare polyoxometalate cluster [NiW12O44]14- based solid as a pre-catalyst for efficient and long-term oxygen evolution.” In: *Nanoscale Adv.* (2022).

[74] Y. Wang et al. “Core–shell-type ZIF-8@ ZIF-67@ POM hybrids as efficient electrocatalysts for the oxygen evolution reaction”. In: *Inorg. Chem. Front.* 6 (2019), pp. 2514–2520.

[75] Y. Wang et al. “PBA@ POM hybrids as efficient electrocatalysts for the oxygen evolution reaction”. In: *Chem. Asian J.* 14 (2019), pp. 2790–2795.

[76] Matthias Steimecke et al. “Higher Valent Nickel Oxides with Improved Oxygen Evolution Activity and Stability in Alkaline Media Prepared by High-Temperature Treatment of Ni(OH) 2”. In: *ACS Catalysis* (Feb. 2020). DOI: 10.1021/acscatal.9b04788.

[77] URL: https://www.alibaba.com/product-detail/99-99-Top-Quality-reduced-graphene_1600233768465.html?spm=a2700.7724857.normal_offer.d_title.166661cdt90BF5 (visited on 01/09/2022).

[78] URL: https://www.alibaba.com/product-detail/Reduced-Graphene-Oxide-Graphene-Oxide-Price_62409775857.html?spm=a2700.galleryofferlist.normal_offer.d_title.257b69cfnj4Her&s=p (visited on 01/09/2022).

[79] URL: https://www.sigmaaldrich.com/PT/en/product/aldrich/805424 (visited on 01/09/2022).

[80] URL: https://www.alibaba.com/product-detail/Ir02-Nanoparticles-Iridium-dioxide-Iridium-Oxide_1600262487085.html?spm=a2700.7724857.normal_offer.d_title.54101b16la2nov (visited on 01/09/2022).

[81] URL: https://www.alibaba.com/product-detail/Iridium-Oxide-Factory-Price-Sell-Nano_62424384729.html?spm=a2700.7724857.normal_offer.d_title.54101b16la2nov&s=p (visited on 01/09/2022).

[82] URL: https://www.sigmaaldrich.com/PT/en/product/aldrich/206237 (visited on 01/09/2022).

[83] URL: https://www.sigmaaldrich.com/PT/en/product/sigma/t2786?gclid=CjOKCQjwhqaVBhCxARIsAHK1tiMMzjS9p23HJNLtL43WcnVADTo-4XuO-JAf7HloecaAqNAEALw_wcB (visited on 01/09/2022).

[84] URL: https://www.sigmaaldrich.com/PT/en/product/sial/p4006 (visited on 01/09/2022).

Appendix A

Annex

Capacitance graphs and impedance graphs for higher potentials are shown in the Annex.

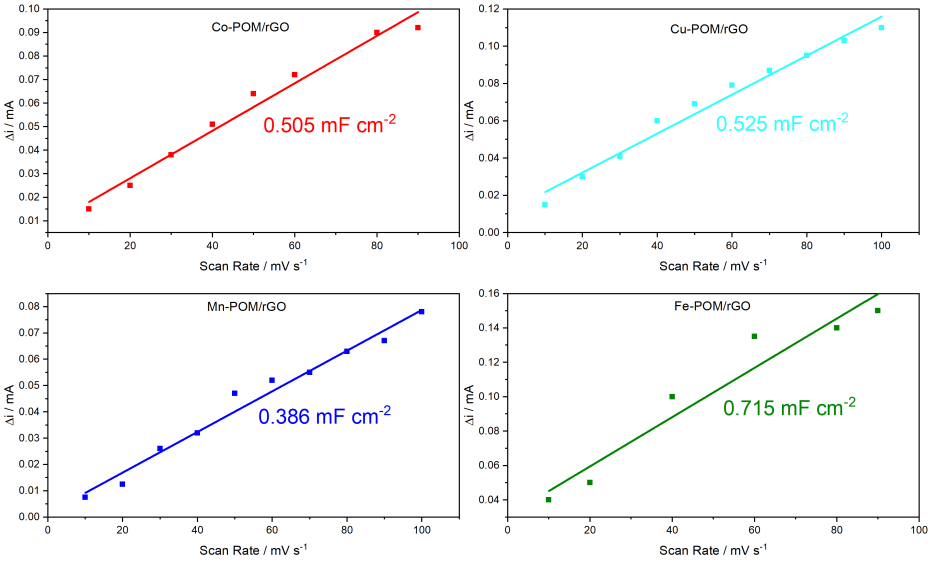

Figure A.1: Difference between cathodic and anodic current density vs. scan rate for Co-POM/rGO (5:1), Cu-POM/rGO (5:1), Fe-POM/rGO (5:1) and Mn-POM/rGO (5:1).

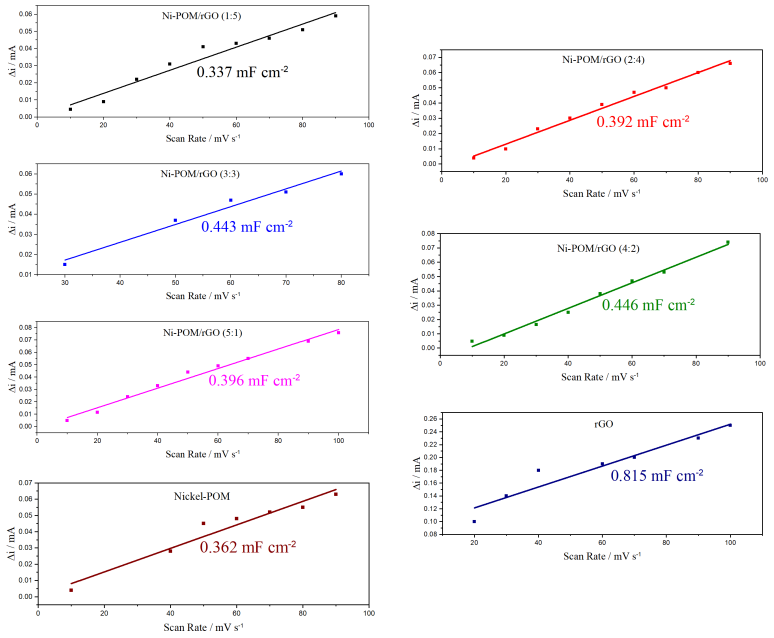

Figure A.2: Difference between cathodic and anodic current density vs. scan rate for IrO_2, rGO and Ni-POM/rGO at different POM:rGO ratios.

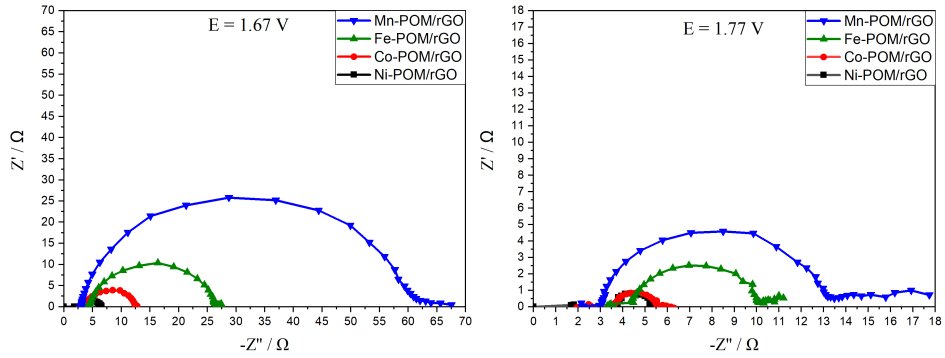

Figure A.3: Nyquist plots of different POM/rGO composites at 1.67 V and 1.77 V.

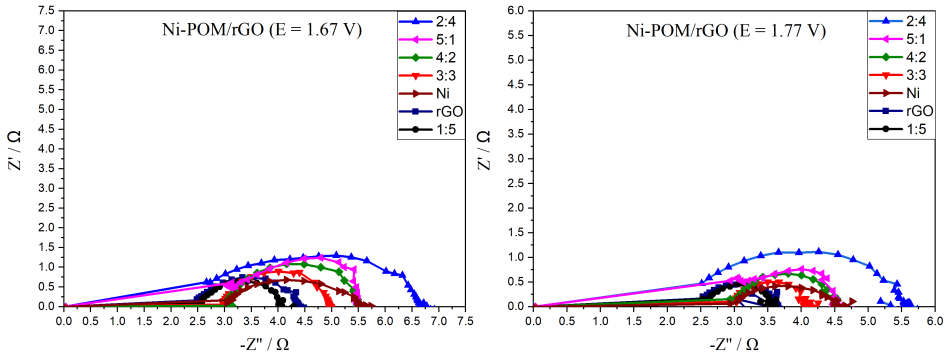

Figure A.4: Nyquist plots of Ni-POM/rGO with different POM:rGO ratios at 1.67 V and 1.77 V.

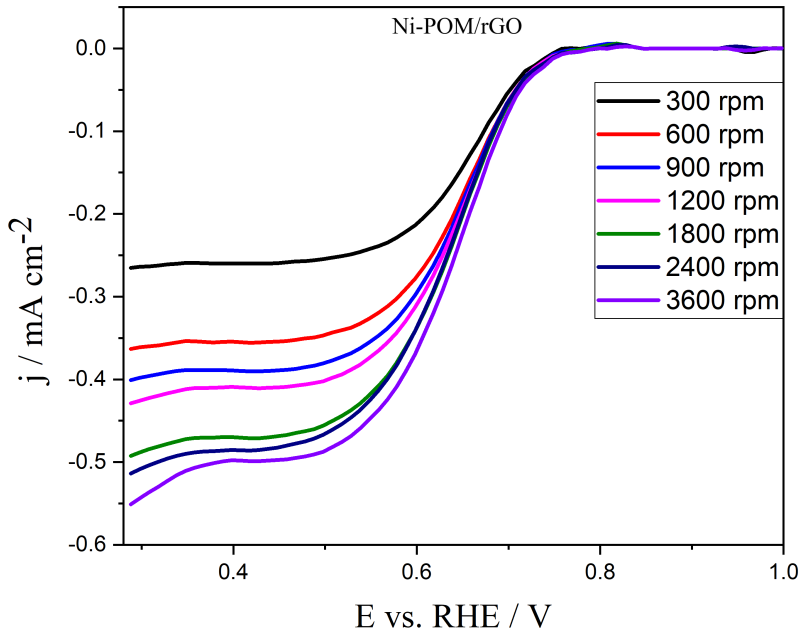

Figure A.5: LSVs for Ni-POM/rGO at different electrode rotation rates.

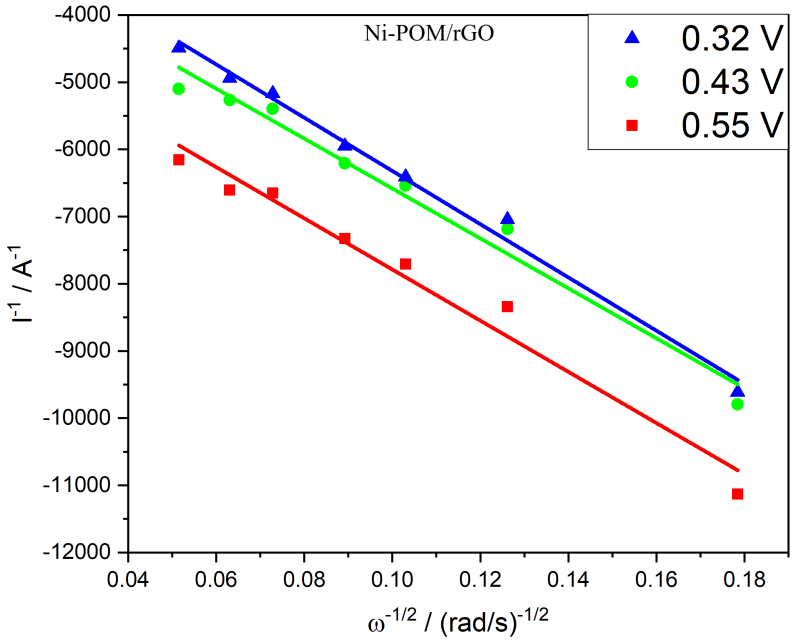

Figure A.6: Koutecky-Levich analysis of Ni-POM/rGO at three different potentials.